
Designing the tapering of a radially oriented flexure joint

BACHELOR THESIS

M. C. Boulogne

Examination Committee

Dr. ir. M. Nijenhuis (committee chair)
Dr. ir. J.S. Kanger (external member)

PRECISION ENGINEERING,
UNIVERSITY OF TWENTE,
29-6-2022

Contents

1	Introduction	2
2	Research question	4
2.1	Main-question	4
2.2	Sub-questions	4
3	Linear analysis	5
3.1	Creating the Linear Model	5
3.1.1	Stiffness Matrix	5
3.1.2	Simplifications and approximations	5
3.1.3	Equilibrium equations	6
3.1.4	Stiffness equations	10
3.1.5	Boundary conditions	11
3.1.6	Rotation of the axis	12
3.1.7	Determining the Stiffness Matrix	13
3.2	Verification of the linear model	16
3.2.1	Stiffness Matrix O-O	16
3.2.2	Stiffness Matrix O-tap	18
3.3	Stress determination from the linear model	21
3.4	Verifying the stresses	23
4	Non-linear Analysis	26
4.1	The shortening effect	26
5	Designing the tapering	27
5.1	Determining the multiplication factor	29
6	Calculating the maximum turning angle	30
7	Conclusion	32
8	Discussion	33
9	Plagiarism check	34
10	Acknowledgement	34
	References	35
A	Analytical calculation of the linear model	1
A.1	Determining of the deformation if $Fz = 0$	1
A.1.1	Deformation in the x-direction	1
A.1.2	Deformation in the y-direction	2
A.2	Turning angle	2
A.3	Rotation of the axis	3
B	Stiffness Matrix $C_{O,O}$	8
C	Full expressions for the stresses derived from the linear model	10

1 Introduction

Flexure mechanisms are widely used in the field of precision engineering to accurately translate or rotate certain objects [1][2][3]. The great advantage of these flexures can be best explained by considering the following traditional case: A stationary object is on top of an arbitrary surface and has to be moved by 1 nanometer. When the object is set into motion the friction between the surface and the object drops rapidly. This causes the object to quickly accelerate and thus creating an overshoot on the desired movement. This effect is called stick-slip. A flexure mechanism solves this problem due to its fully elastic deformation. Because of this, there are no rolling or sliding contacts, no backlash and no stick-slip. This causes the behaviour of a flexure to be very predictable and relatively easy to describe with the help of elasticity theory. With this, the flexure has the ability to accurately translate or rotate an object in one direction while maintaining high stiffness in other directions. Although this elastic property gives the flexure a very predictable behavior, it also limits the range of motion. This then also limits the range of possible applications.

Flexure mechanisms mostly consist of a main stage which can be accurately rotated or translated due to the various elastic components attached to it. The configurations of these elastic components influence the motion of the main stage. The components provide low stiffness in the direction of the desired motion while maintaining high stiffness in other directions.

The radially oriented flexure joint seen in figure 1 is the focus of this research. The bottom plate is grounded and there is an external moment exerted on the top plate making it rotate about the z -axis. The top and bottom plate are connected with several leaf-springs that are placed along the radial axis of the plates. This greatly reduces the mobility of the top plate in all directions apart from the rotation about the z -axis. A more clear representation of the movement of the flexure can be seen in figure 2.

Although this flexure has great potential, there is one big issue: The stress in the leaf-springs increases quickly with an increasing angle about the z -axis. When the angle reaches its critical value, the stress in the tapering will be so high that the flexure mechanism starts to deform plastically. This means that the flexure will permanently deform, making it lose all of its application purposes.

An example for a possible application of this flexure mechanism is the Mid-infrared ELT Imager and Spectrograph (METIS) instrument for the Extremely Large Telescope (ELT) of the European Southern Observatory (ESO)[4]. METIS is used for researching proto planetary disks, the formation of our Solar System, the growth of supermassive black holes and the dynamics of high- z galaxies. To perform accurate measurements, it is important that the effects of the rotation of the earth are cancelled out. Currently, this is done with a conventional bearing. With the radially oriented flexure joint, the bearing could be replaced to more accurately cancel out this rotation effect. It is preferred that the consecutive time in which measurements can be done, is as long as possible. Because of this the maximum turning angle of the flexure has to be as high as possible. The more the flexure can be turned, the longer the effects of the rotation of the earth can be cancelled out.

In this report, it will be researched how to increase this critical angle, after which the flexure starts to deform plastically. This will be done by designing the tapering such that the maximum stress for a certain turning angle in the flexure is as low as possible. The first step to do this, is to create a linear model that describes the forces and moments in the flexure mechanism as a function of the input displacement about the origin. From this model, it can be determined in what directions the flexure will deform when certain input forces and moments are given. Also the basis for the stress analysis can be derived from the model. The next step will be to take a look at which non-linear effects have a big influence on the stresses in the leaf-springs. With the equations describing these effects and the results from the linear model, a design for the tapering in the radially oriented flexure joint can be created.

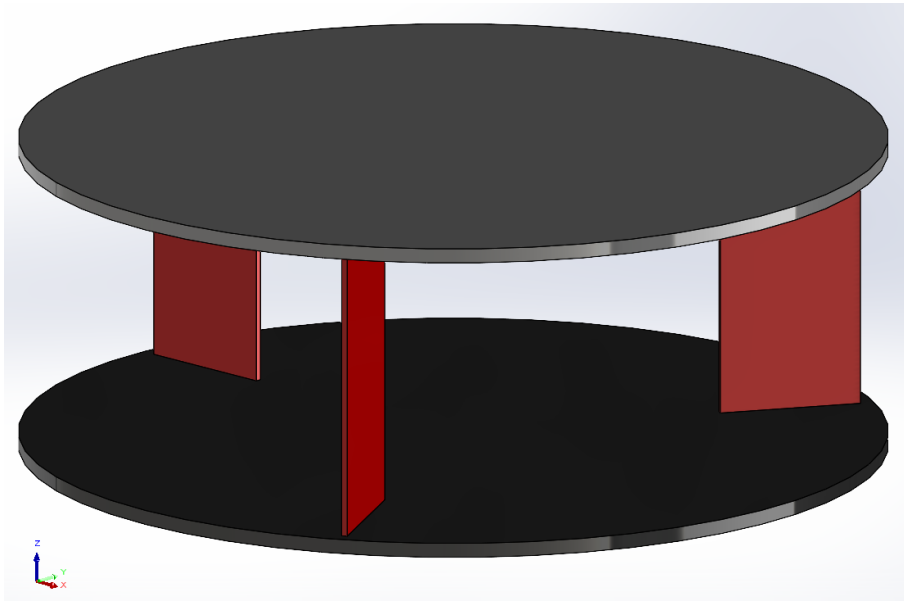


Figure 1: The radially oriented flexure joint. The joint consist of the bottom plate (black), the tapering (red) and the top plate (grey).

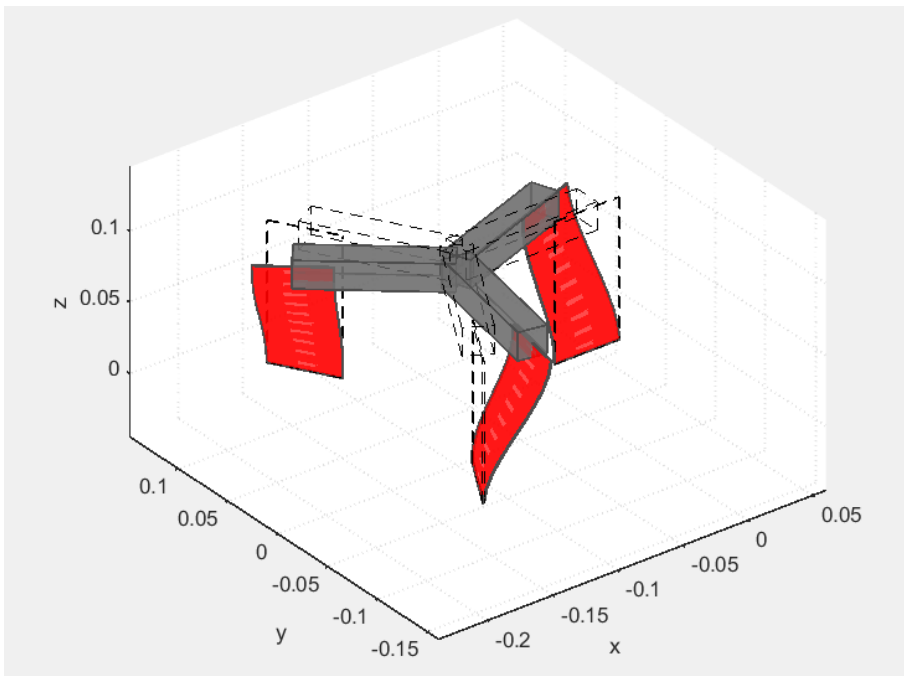


Figure 2: A depiction of the movement of the radially oriented flexure joint.

2 Research question

2.1 Main-question

What design of the tapering in the radially oriented flexure joint seen in figure 1, will have the largest possible turn angle about the z -axis before the critical stress in the flexure mechanism is achieved?

2.2 Sub-questions

- Which linear analytical expression can be used to describe the forces and moments as a function of the displacement and rotation in the radially oriented flexure joint?
- What are the stresses that result from linear effects in the radially oriented flexure joint as a function of the displacement and rotation?
- What non-linear effects have a significant influence on the stresses in the leaf-springs of the radially oriented flexure joint?
- How much can the possible turn angle about the z -axis of the radially oriented flexure joint be increased by redesigning the shape of the tapering?

3 Linear analysis

In the first part of this report, the linear analysis of the flexure mechanism will be described. In this linear analysis, a linear model will be derived that gives the forces and moments in the flexure as a function of the displacement and rotation. After the validity of this model has been verified, the stresses due to the linear effects will be derived from it. It will then be inspected when these stresses give a valid representation of the stresses in the linear model.

3.1 Creating the Linear Model

In this section the linear model of the forces and moments in the flexure as a function of the displacement and rotation about the origin will be derived. This linear model will be the basis for the analysis of the flexure mechanism. The global displacements of the flexure can be quickly seen from this model. Also the first approximation for the stresses in the tapering can be derived from the model.

3.1.1 Stiffness Matrix

From [5] it can be seen that in a linear model the displacements and rotations of an arbitrary point are related to the forces and moments of another arbitrary point according to the following equation:

$$\vec{r} = \mathbf{C}\vec{F} \quad (1)$$

where \vec{r} is the displacement and rotation vector given by $\vec{r} = \begin{pmatrix} u_x \\ u_y \\ u_z \\ \phi_x \\ \phi_y \\ \phi_z \end{pmatrix}$, where \vec{F} is the forces and moments vector given by $\vec{F} = \begin{pmatrix} F_x \\ F_y \\ F_z \\ M_x \\ M_y \\ M_z \end{pmatrix}$

and \mathbf{C} is the stiffness matrix which combines the two vectors. The elements of a stiffness matrix are numbered according to the

following matrix: $\mathbf{C} = \begin{pmatrix} A_1 & A_2 & A_3 & A_4 & A_5 & A_6 \\ B_1 & B_2 & B_3 & B_4 & B_5 & B_6 \\ C_1 & C_2 & C_3 & C_4 & C_5 & C_6 \\ D_1 & D_2 & D_3 & D_4 & D_5 & D_6 \\ E_1 & E_2 & E_3 & E_4 & E_5 & E_6 \\ F_1 & F_2 & F_3 & F_4 & F_5 & F_6 \end{pmatrix}$

The stiffness matrices will be derived in the rest of this section by simplifying the flexure, setting up the equilibrium equations, determining the stiffness equations, determining the boundary conditions and finally merging all these equations together.

3.1.2 Simplifications and approximations

The first step is to simplify this flexure. The top plate will be simplified to a set of rigid beams that can not deform. The tapering will be seen as a beam that can deform and is grounded at its bottom plate. The simplification can be seen in figure 3.

It will also be assumed that the tapering in the flexure will deform according to Euler-Bernoulli beam theory[6]. For this beam theory, it is assumed that the displacement is small enough such that every point on the neutral line of a beam only moves in the transverse direction and that this transverse displacement is the same for all points in a cross section throughout the beam. Due to this small displacement linear approximations are also valid.

The final assumption that will be made is that the effects of shear in the flexure are sufficiently small, such that they can be neglected. This assumption is made to increase the simplicity of the model. If the width of the leaf-springs is small enough compared to the height of the flexure, then these shear effects should indeed be negligible.

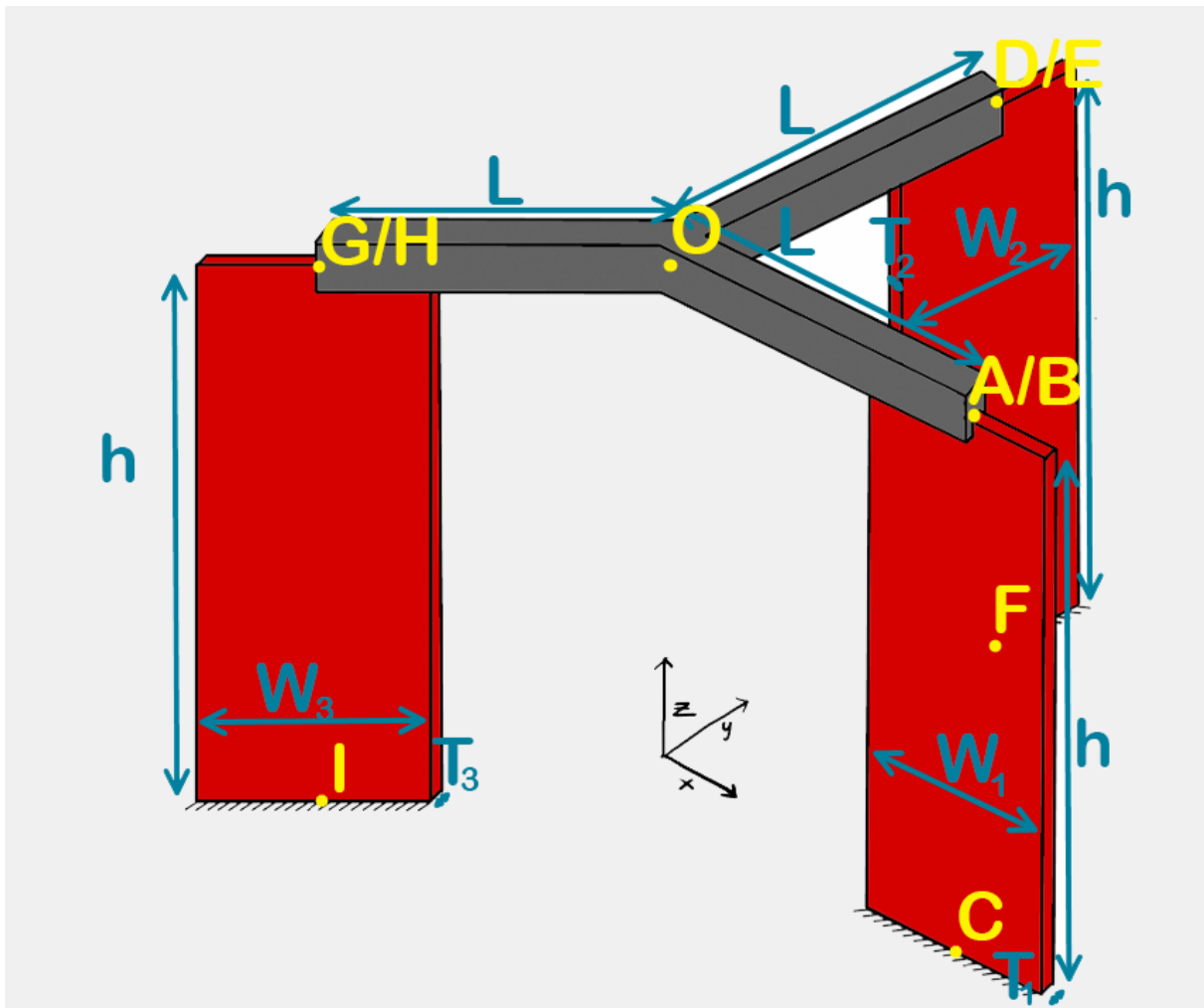


Figure 3: The simplification of the flexure joint. At the top three rigid beams (grey) and below the flexible beams that are grounded (red), together with the dimensions (blue) and the important points (yellow).

3.1.3 Equilibrium equations

The equilibrium equations give the relations of the forces and moments between connected points in the flexure mechanism. These relations are needed for the computation of the stiffness matrix.

A schematic overview of the forces and moments that act throughout the beams that are aligned with the x -axis can be seen in figures 4-6. The forces and moments that act on the rigid beam are shown in figure 4 and the forces and moments that act on the corresponding flexible beam are shown in figure 5. In figure 6 the forces and moments throughout these beams can be seen in the 2D cross sections.

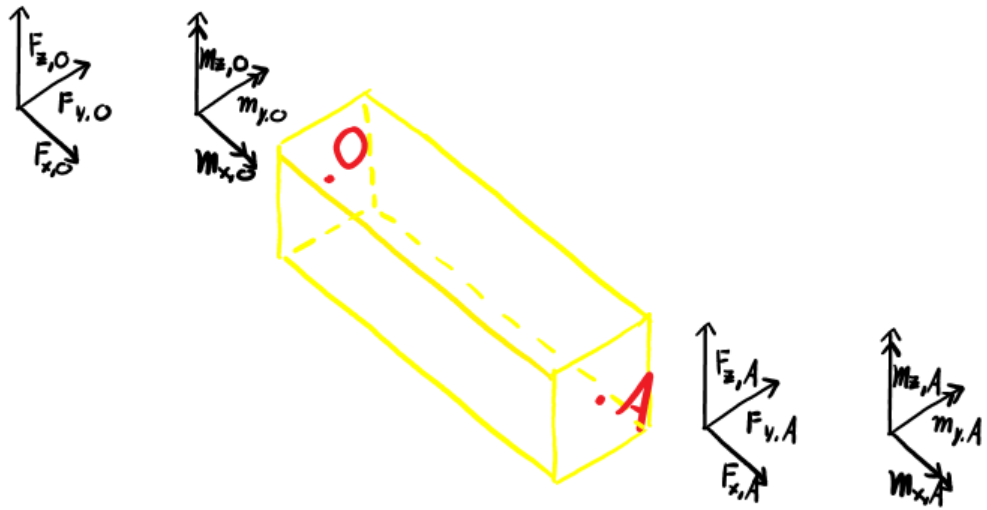


Figure 4: The forces and moments that act on the rigid beam that is aligned with the x -axis.

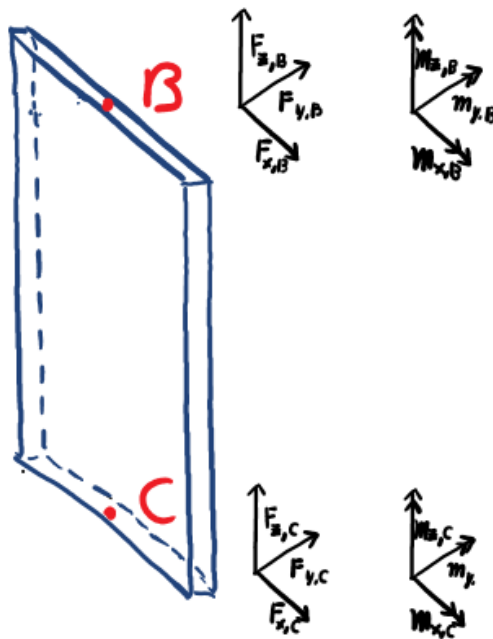


Figure 5: The forces and moments that act on the flexible beam that is aligned with the x -axis.

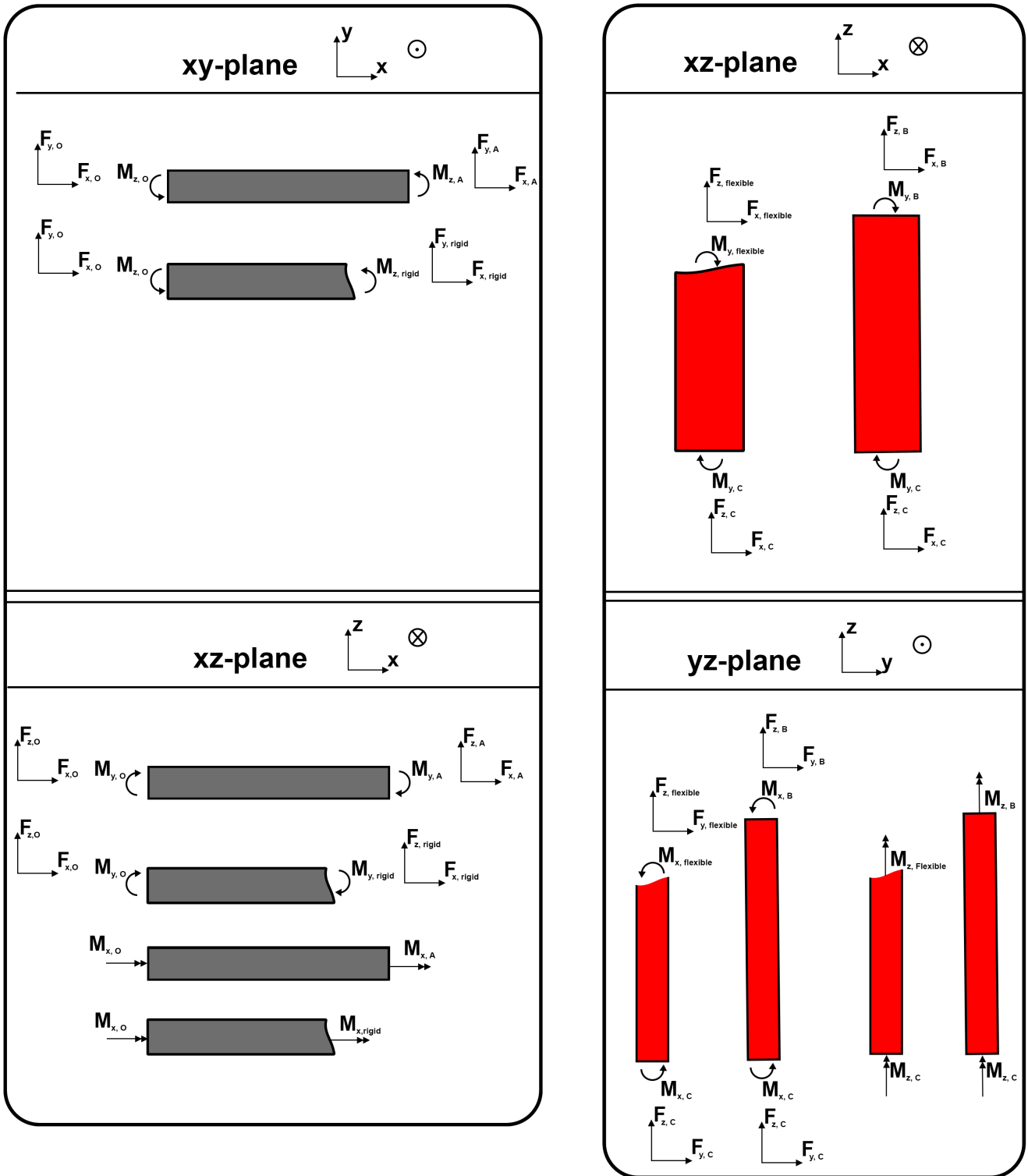


Figure 6: The sketches of the cross sections of the beams seen in figure 4 and 5. In these sketches the forces and moments are also included.

From these sketches the equilibrium equations of the flexure can be derived. If the forces and moments in point O are coupled with:

$$F_{x,O} = F_{1,x,O} + F_{2,x,O} + F_{3,x,O} \quad (2)$$

$$F_{y,O} = F_{1,y,O} + F_{2,y,O} + F_{3,y,O} \quad (3)$$

$$F_{z,O} = F_{1,z,O} + F_{2,z,O} + F_{3,z,O} \quad (4)$$

$$M_{x,O} = M_{1,x,O} + M_{2,x,O} + M_{3,x,O} \quad (5)$$

$$M_{y,O} = M_{1,y,O} + M_{2,y,O} + M_{3,y,O} \quad (6)$$

$$M_{z,O} = M_{1,z,O} + M_{2,z,O} + M_{3,z,O} \quad (7)$$

then the forces and moments in the rigid beam are given by:

$$F_{1,x,O} = -F_{x,A} = -F_{x,rigid} \quad (8)$$

$$F_{1,y,O} = -F_{y,A} = -F_{y,rigid} \quad (9)$$

$$F_{1,z,O} = -F_{z,A} = -F_{z,rigid} \quad (10)$$

$$M_{1,z,O} = -M_{z,A} - (L + f_x(L))F_{y,A} + f_y(L)F_{x,A} \quad (11)$$

$$M_{1,z,O} = -M_{z,rigid} - (x + f_x(x))F_{y,rigid} + f_y(x)F_{x,rigid} \quad (12)$$

$$M_{1,y,O} = -M_{y,A} + (L + f_x(L))F_{z,A} + f_z(L)F_{x,A} \quad (13)$$

$$M_{1,y,O} = -M_{y,rigid} + (x + f_x(x))F_{z,rigid} + f_z(x)F_{x,rigid} \quad (14)$$

$$M_{1,x,O} = -M_{x,A} - f_y(L)F_{z,A} + f_z(L)F_{y,A} \quad (15)$$

$$M_{1,x,O} = -M_{x,rigid} - f_y(x)F_{z,rigid} + f_z(x)F_{y,rigid} \quad (16)$$

Here L is the length, $f_x(x)$ is the function that gives the displacement of the x -axis, $f_y(x)$ is the function that gives the displacement of the y -axis and $f_z(x)$ is the function that gives the displacement of the z -axis of the rigid beam.

Because the beam is rigid, it is known that $f_x(x) = f_y(x) = f_z(x) = 0$. With this the equations can be simplified as:

$$M_{1,z,O} = -M_{z,A} - LF_{y,A} \quad (17)$$

$$M_{1,z,O} = -M_{z,rigid} - xF_{y,rigid} \quad (18)$$

$$M_{1,y,O} = -M_{y,A} + LF_{z,A} \quad (19)$$

$$M_{1,y,O} = -M_{y,rigid} + xF_{z,rigid} \quad (20)$$

$$M_{1,x,O} = -M_{x,A} \quad (21)$$

$$M_{1,x,O} = -M_{x,rigid} \quad (22)$$

Due to the third law of Newton [6], the forces and moments in point A are the opposite of the forces and moments in point B. From this it follows that these forces and moments are coupled with the following equations:

$$F_{x,B} = -F_{x,A} \quad (23)$$

$$F_{y,B} = -F_{y,A} \quad (24)$$

$$F_{z,B} = -F_{z,A} \quad (25)$$

$$M_{x,B} = -M_{x,A} \quad (26)$$

$$M_{y,B} = -M_{y,A} \quad (27)$$

$$M_{z,B} = -M_{z,A} \quad (28)$$

From the cross-sections, the equations for the forces and moments in the flexible beam can also be derived:

$$F_{x,B} = -F_{x,C} = F_{x,flexible} \quad (29)$$

$$F_{y,B} = -F_{y,C} = F_{y,flexible} \quad (30)$$

$$F_{z,B} = -F_{z,C} = F_{z,flexible} \quad (31)$$

$$M_{x,B} = -M_{x,C} + (h + u_z(h))F_{y,B} - u_y(h)F_{z,B} \quad (32)$$

$$M_{x,flexible} = -M_{x,C} + (z + u_z(z))F_{y,flexible} - u_y(z)F_{z,flexible} \quad (33)$$

$$M_{x,,flexible} = -M_{x,C} + (z + u_z(z))F_{y,B} - u_y(z)F_{z,B} \quad (34)$$

$$M_{y,B} = -M_{y,C} - (h + u_z(h))F_{x,B} + u_x(h)F_{z,B} \quad (35)$$

$$M_{y,flexible} = -M_{y,C} - (z + u_z(z))F_{x,flexible} + u_x(z)F_{z,flexible} \quad (36)$$

$$M_{y,flexible} = -M_{y,C} - (z + u_z(z))F_{x,B} + u_x(z)F_{z,B} \quad (37)$$

$$M_{z,B} = -M_{z,C} + u_y(h)F_{x,B} - u_x(h)F_{y,B} \quad (38)$$

$$M_{z,flexible} = -M_{z,C} + u_y(z)F_{x,flexible} - u_x(z)F_{y,flexible} \quad (39)$$

$$M_{z,,flexible} = -M_{z,C} + u_y(z)F_{x,B} - u_x(z)F_{y,B} \quad (40)$$

Here h is the height, $u_x(z)$ is the function that gives the displacement of the x -axis, $u_y(z)$ gives the displacement of the y -axis and $u_z(z)$ gives the displacement of the z -axis of the flexible beam.

Several linear approximations can be made in equations 32-40. The terms with $u_x(z)$, $u_y(z)$ and $u_z(z)$ are significantly smaller than the rest. These terms can therefore be approximated to zero in the linear analysis. This results in the following simplified equilibrium equations:

$$M_{x,B} = -M_{x,C} + hF_{y,B} \quad (41)$$

$$M_{x,flexible} = -M_{x,C} + zF_{y,flexible} \quad (42)$$

$$M_{x,flexible} = -M_{x,C} + zF_{y,B} \quad (43)$$

$$M_{y,B} = -M_{y,C} - hF_{x,B} \quad (44)$$

$$M_{y,flexible} = -M_{y,C} - zF_{x,flexible} \quad (45)$$

$$M_{y,flexible} = -M_{y,C} - zF_{x,B} \quad (46)$$

$$M_{z,B} = -M_{z,C} \quad (47)$$

$$M_{z,flexible} = -M_{z,C} \quad (48)$$

With this the equilibrium equations are derived and linearly approximated.

3.1.4 Stiffness equations

With the stiffness equations, the earlier derived equilibrium equations can be coupled to the deformations and rotations in the flexure. These stiffness equations can be derived from [1] with the earlier mentioned assumptions that the leaf-springs deform according to Euler-Bernoulli beam theory and that the shear effects can be neglected.

The strain and curvature can be determined from the displacement and rotation with the following equations:

$$\kappa_x(s) = \phi'_x = -u''_y \quad (49)$$

$$\kappa_y(s) = \phi'_y = u''_x \quad (50)$$

$$\kappa_z(s) = \phi'_z \quad (51)$$

$$\gamma_y(s) = 0 \quad (52)$$

$$\gamma_x(s) = 0 \quad (53)$$

$$\gamma_z(s) = u'_z \quad (54)$$

$$(55)$$

Here, $u_x, u_y, u_z, \phi_x, \phi_y$ and ϕ_z are the deformations in the leaf-spring.

To couple these strains and curvatures to the forces and moments, the constitutive relations can be used. These are given by:

$$F_{z,flexible} = EA\gamma_z \quad (56)$$

$$M_{x,flexible} = EI_x\kappa_x \quad (57)$$

$$M_{y,flexible} = EI_y\kappa_y \quad (58)$$

$$M_{z,flexible} = GJ\kappa_z \quad (59)$$

Here, E is the elasticity modulus, G is the shear modulus, A is the cross-sectional area given by:

$$A = wt \quad (60)$$

where w is the width and t is the thickness of the beam,

I_x is the moment of inertia about the x -axis which is given by [6]:

$$I_x = \int y^2 dA \quad (61)$$

I_y is the moment of inertia about the y -axis which is given by: [6]

$$I_y = \int x^2 dA \quad (62)$$

and J is the torsional constant. If the beam is sufficiently thin, so $t \ll w$, then the torsional constant can be calculated with[3]:

$$J = \frac{1}{3}wt^3 \quad (63)$$

With this all the stiffness equations necessary for the linear model have been drawn up.

3.1.5 Boundary conditions

The last set of equations needed for the stiffness matrix are the boundary conditions. These conditions give the deformations at the top and bottom of the tapering.

The boundary conditions for the flexible beam that is aligned with the x -axis can be determined from the location of point A/B and point C (see figure 3).

It is assumed that the center (point O) is translated and rotated with the following vector:

$$\vec{r} = \begin{pmatrix} \Delta_x \\ \Delta_y \\ \Delta_z \\ \theta_x \\ \theta_y \\ \theta_z \end{pmatrix} \quad (64)$$

Because the top beam is rigid, the movement of point A/B and point C is coupled with kinematic relations to that of point O. It then follows from simple geometry that the positions of point A/B and point C are:

$$P_{A/B} = \begin{pmatrix} u_x(z=h) + L \\ u_y(z=h) \\ u_z(z=h) + h \\ \phi_x(z=h) \\ \phi_y(z=h) \\ \phi_z(z=h) \end{pmatrix} = \begin{pmatrix} L \\ 0 \\ h \\ 0 \\ 0 \\ 0 \end{pmatrix} + \begin{pmatrix} \Delta_x - 2L \sin(\frac{\theta_z}{2}) \sin(\frac{\theta_z}{2}) (\cos(\theta_y)) \\ \Delta_y + 2L \cos(\frac{\theta_z}{2}) \sin(\frac{\theta_z}{2}) (\cos(\theta_x)) \\ \Delta_z + L \sin(\theta_y) + L \sin(\theta_x) \\ \theta_x \\ \theta_y \\ \theta_z \end{pmatrix} \approx \begin{pmatrix} L + \Delta_x \\ \Delta_y + L\theta_z \\ h + \Delta_z + L\theta_x + L\theta_y \\ \theta_x \\ \theta_y \\ \theta_z \end{pmatrix} \quad (65)$$

$$\vec{p}_C = \begin{pmatrix} u_x(z=0) + L \\ u_y(z=0) \\ u_z(z=0) \\ \phi_x(z=0) \\ \phi_y(z=0) \\ \phi_z(z=0) \end{pmatrix} = \begin{pmatrix} L \\ 0 \\ 0 \\ 0 \\ 0 \\ 0 \end{pmatrix} \quad (66)$$

This results in the following boundary conditions:

$$\begin{pmatrix} u_x(z=0) \\ u_y(z=0) \\ u_z(z=0) \\ \phi_x(z=0) \\ \phi_y(z=0) \\ \phi_z(z=0) \end{pmatrix} = \begin{pmatrix} 0 \\ 0 \\ 0 \\ 0 \\ 0 \\ 0 \end{pmatrix} \quad \text{and} \quad \begin{pmatrix} u_x(z=h) \\ u_y(z=h) \\ u_z(z=h) \\ \phi_x(z=h) \\ \phi_y(z=h) \\ \phi_z(z=h) \end{pmatrix} = \begin{pmatrix} \Delta_x - 2L \sin(\frac{\theta_z}{2}) \sin(\frac{\theta_z}{2}) (\cos(\theta_y)) \\ \Delta_y + 2L \cos(\frac{\theta_z}{2}) \sin(\frac{\theta_z}{2}) (\cos(\theta_x)) \\ \Delta_z + L \sin(\theta_y) + L \sin(\theta_x) \\ \theta_x \\ \theta_y \\ \theta_z \end{pmatrix} \approx \begin{pmatrix} \Delta_x \\ \Delta_y + L\theta_z \\ \Delta_z + L\theta_x + L\theta_y \\ \theta_x \\ \theta_y \\ \theta_z \end{pmatrix} \quad (67)$$

3.1.6 Rotation of the axis

With the now simplified equilibrium, stiffness and boundary equations the forces, moments, displacements and rotations of the rigid and flexible beam that are aligned with the x -axis can be derived. For the stiffness matrices the forces and moments in the beams that are not aligned with the x -axis also need to be determined. This can be done by drawing up new equilibrium, stiffness and boundary equations for all of these beams. However, due to the symmetry of the flexure it can also be done a lot easier.

If first the forces, moments, displacements and rotations of each beam are determined in a coordinate system where the beam is aligned with its "own" x -axis (see figure 7). Then the remaining equations can be determined by simply rotating these new coordinate systems to the original coordinate system. The coordinate systems denoted by (x'_2, y'_2) and (x'_3, y'_3) can be rotated to and from the original coordinate system by applying the following rotation matrices:

$$\begin{pmatrix} x'_2 \\ y'_2 \end{pmatrix} = \begin{pmatrix} \cos(\alpha) & \sin(\alpha) \\ -\sin(\alpha) & \cos(\alpha) \end{pmatrix} \begin{pmatrix} x \\ y \end{pmatrix} = \begin{pmatrix} -\frac{1}{2} & \frac{\sqrt{3}}{2} \\ -\frac{\sqrt{3}}{2} & -\frac{1}{2} \end{pmatrix} \begin{pmatrix} x \\ y \end{pmatrix} \quad (68)$$

$$\begin{pmatrix} x'_3 \\ y'_3 \end{pmatrix} = \begin{pmatrix} \cos(2\alpha) & \sin(2\alpha) \\ -\sin(2\alpha) & \cos(2\alpha) \end{pmatrix} \begin{pmatrix} x \\ y \end{pmatrix} = \begin{pmatrix} -\frac{1}{2} & -\frac{\sqrt{3}}{2} \\ \frac{\sqrt{3}}{2} & -\frac{1}{2} \end{pmatrix} \begin{pmatrix} x \\ y \end{pmatrix} \quad (69)$$

$$\begin{pmatrix} x \\ y \end{pmatrix} = \begin{pmatrix} \cos(2\alpha) & \sin(2\alpha) \\ -\sin(2\alpha) & \cos(2\alpha) \end{pmatrix} \begin{pmatrix} x'_2 \\ y'_2 \end{pmatrix} = \begin{pmatrix} -\frac{1}{2} & -\frac{\sqrt{3}}{2} \\ \frac{\sqrt{3}}{2} & -\frac{1}{2} \end{pmatrix} \begin{pmatrix} x'_2 \\ y'_2 \end{pmatrix} \quad (70)$$

$$\begin{pmatrix} x \\ y \end{pmatrix} = \begin{pmatrix} \cos(\alpha) & \sin(\alpha) \\ -\sin(\alpha) & \cos(\alpha) \end{pmatrix} \begin{pmatrix} x'_3 \\ y'_3 \end{pmatrix} = \begin{pmatrix} -\frac{1}{2} & \frac{\sqrt{3}}{2} \\ -\frac{\sqrt{3}}{2} & -\frac{1}{2} \end{pmatrix} \begin{pmatrix} x'_3 \\ y'_3 \end{pmatrix} \quad (71)$$

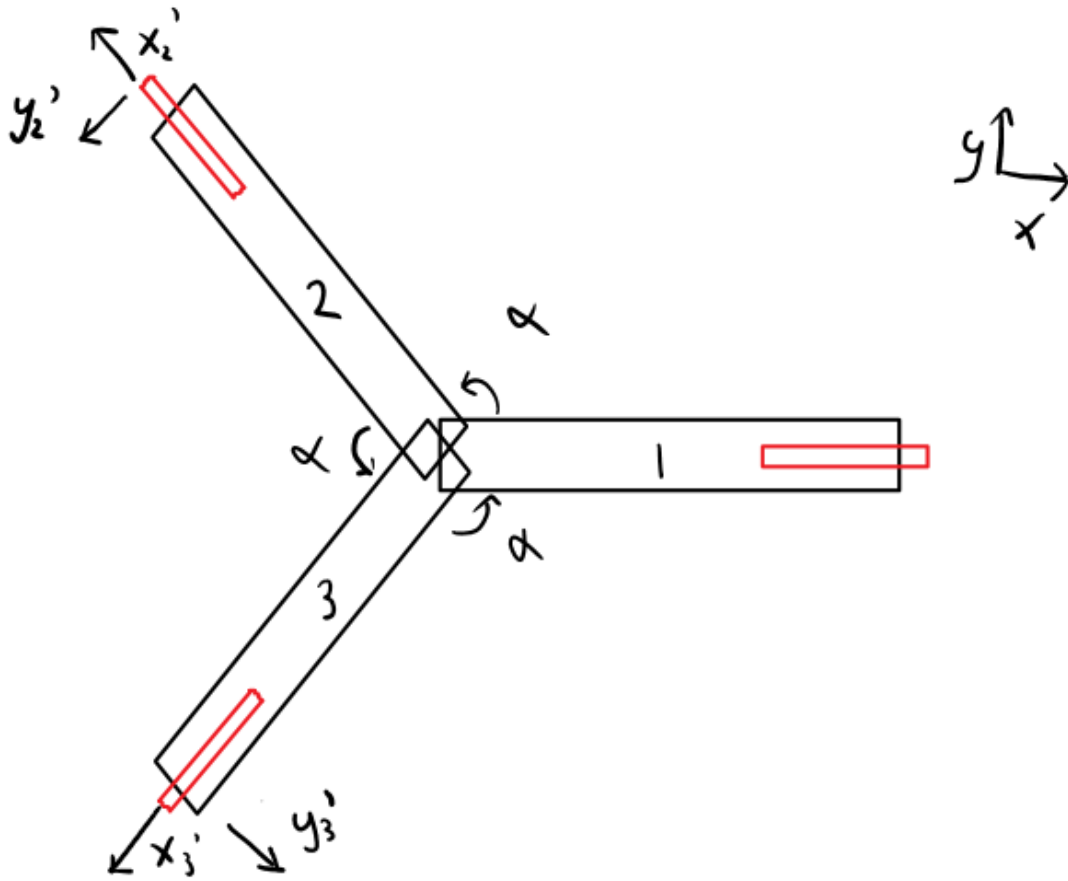


Figure 7: A schematic depiction of the axis rotation. The axes are rotated by an angle α or 2α , to form the rotated coordinate systems (x'_2, y'_2) and (x'_3, y'_3) .

If these rotation matrices are implemented into the equations that couple the forces and moments in point O (eq 2-7). Then these equations can be rewritten as:

$$F_{x,o} = F_{1,x,o} - \frac{1}{2}F_{2,x'_2,o} + \frac{\sqrt{3}}{2}F_{2,y'_2,o} - \frac{1}{2}F_{3,x'_3,o} - \frac{\sqrt{3}}{2}F_{3,y'_3,o} \quad (72)$$

$$F_{y,o} = F_{1,y,o} - \frac{\sqrt{3}}{2}F_{2,x'_2,o} - \frac{1}{2}F_{2,y'_2,o} + \frac{\sqrt{3}}{2}F_{3,x'_3,o} - \frac{1}{2}F_{3,y'_3,o} \quad (73)$$

$$F_{z,o} = F_{1,z,o} + F_{2,z,o} + F_{3,z,o} \quad (74)$$

$$M_{x,o} = M_{1,x,o} - \frac{1}{2}M_{2,x'_2,o} + \frac{\sqrt{3}}{2}M_{2,y'_2,o} - \frac{1}{2}M_{3,x'_3,o} - \frac{\sqrt{3}}{2}M_{3,y'_3,o} \quad (75)$$

$$M_{y,o} = M_{1,y,o} - \frac{\sqrt{3}}{2}M_{2,x'_2,o} - \frac{1}{2}M_{2,y'_2,o} + \frac{\sqrt{3}}{2}M_{3,x'_3,o} - \frac{1}{2}M_{3,y'_3,o} \quad (76)$$

$$M_{z,o} = M_{1,z,o} + M_{2,z,o} + M_{3,z,o} \quad (77)$$

With this, all the necessary equations for the determination of the stiffness matrix have been drawn up.

3.1.7 Determining the Stiffness Matrix

With the derived equilibrium, stiffness and boundary equations (eq. 8-10, 17-31 and 49-77) the stiffness matrices can be determined. The calculations for this are done in Wolfram Mathematica and are therefore not described in this chapter. These analytical calculations can be seen in Appendix A.

The stiffness matrix couples the displacements and rotations of an arbitrary point to the forces and moments of another arbitrary point according to equation 1. In this chapter two stiffness matrices will be calculated; the stiffness matrix which couples

the displacements and rotations to the forces and moments of point O and the stiffness matrix that couples the displacements and rotations of point O to the forces and moments in the tapering.

With these stiffness matrices, it can be derived what the general deformation of the flexure and what the stress due to the linear effects will be.

The first relation that is looked at, is the relation between the forces and moments and the displacements and rotations of point O. This relation can be examined with the corresponding stiffness matrix. The resulting matrix is however very big and can therefore, for readability purposes, only be seen in appendix B. If the assumption is made that the width and length of all three leaf-springs are the same, then the stiffness matrix can be simplified to:

$$C_{O,O} = \begin{pmatrix} \frac{18E(I_x+I_y)}{h^3} & 0 & 0 & 0 & -\frac{9E(I_x+I_y)}{h^2} & 0 \\ 0 & \frac{18E(I_x+I_y)}{h^3} & 0 & \frac{9E(I_x+I_y)}{h^2} & 0 & 0 \\ 0 & 0 & \frac{3AE}{h} & 0 & 0 & 0 \\ 0 & \frac{9E(I_x+I_y)}{h^2} & 0 & \frac{3E(AL^2+4(I_x+I_y)h)}{2h} & -\frac{3AEL^2}{2h} & 0 \\ -\frac{9E(I_x+I_y)}{h^2} & 0 & 0 & \frac{3AEL^2}{2h} & \frac{3E(AL^2+4(I_x+I_y))}{2h} & 0 \\ 0 & 0 & 0 & 0 & 0 & \frac{3GJh^2+36EI_xL^2}{h^3} \end{pmatrix} \quad (78)$$

From this matrix together with equation 1, it can be seen that in the linear case, if the width and length of all three leaf-springs is the same, only the moment about the z -axis has an influence on the angle about the z -axis.

To get a better feel for the magnitude of each of the elements in the matrix, representative values can be filled in for the constants. With the following constants: $t = 0.002\text{m}$, $w = 0.05\text{m}$, $L = 0.15\text{m}$, $h = 0.2\text{m}$, $G = 70\text{GPa}$ and $E = 210\text{GPa}$, the stiffness matrix becomes:

$$C_{O,O} = \begin{pmatrix} 4.92384 & 0 & 0 & 0 & -0.492384 & 0 \\ 0 & 4.92384 & 0 & 0.492384 & 0 & 0 \\ 0 & 0 & 157.5 & 0 & 0 & 0 \\ 0 & 0.492384 & 0 & 1.83753 & -1.77188 & 0 \\ -0.492384 & 0 & 0 & 1.77188 & 1.83753 & 0 \\ 0 & 0 & 0 & 0 & 0.000106094 & 0 \end{pmatrix} * 10^6 \quad (79)$$

From the fact that element F_6 is so much smaller than the others it can be seen that the stiffness is by far the lowest in this desired rotational z -direction. This means that the flexure will deform the easiest in this desired direction. Even if there are forces and moments that work in undesired directions, then this will only result in very small deformation in these directions. This makes the flexure well behaved and suitable for its application as a bearing. Because the deformation in all directions apart from the desired direction about the z -axis is very small, the approximation is made that the deformation in all other directions is zero. This approximation will be used in the rest of the report. The high value of element C3 gives that the flexure will deform even less in the z -direction. This means that high amounts of load can be applied in the z -direction while still remaining to have little to none deformation in this direction. This also makes the flexure suitable for its application purposes.

It has been derived that if the dimensions of all three leaf-springs is the same that then the flexure behaves very appropriately for its application purposes. Because of this the design decision is made to keep the dimensions of all three leaf-springs the same for the rest of the report. This means that $w_1 = w_2 = w_3 = w$ and $t_1 = t_2 = t_3 = t$. Which also results in $I_{x,1} = I_{x,2} = I_{x,3} = I_x$, $I_{y,1} = I_{y,2} = I_{y,3} = I_y$ and $J_1 = J_2 = J_3 = J$.

To determine the stresses in the leaf-spring, the forces and moments in this leaf-spring need to be derived. For this the stiffness matrix that couples the displacement and rotation of point O to the forces and moments in one of the leaf-springs is derived. This

stiffness matrix is given by:

$$C_{O,r_f} = \begin{pmatrix} \frac{12EI_y}{h^3} & 0 & 0 & 0 & -\frac{6EI_y}{h^2} & 0 \\ 0 & \frac{12EI_x}{h^3} & 0 & \frac{6EI_x}{h^2} & 0 & \frac{12EI_x L}{h^3} \\ 0 & 0 & \frac{AE}{h} & \frac{AEL}{h} & \frac{AEL}{h} & 0 \\ 0 & -\frac{6EI_x(h-2z)}{h^3} & 0 & -\frac{2EI_x(h-3z)}{h^2} & 0 & -\frac{6EI_x L(h-2z)}{h^3} \\ \frac{6EI_y(h-2z)}{h^3} & 0 & 0 & 0 & -\frac{2EI_y(h-3z)}{h^2} & 0 \\ 0 & 0 & 0 & 0 & 0 & \frac{GJ}{h} \end{pmatrix} \quad (80)$$

With this the, linear model which couples the displacement and rotation to the forces and moments in the leaf-spring has been completed. The movement of the flexure has been derived from this model.

3.2 Verification of the linear model

In this section the earlier derived stiffness matrices will be verified. This will be done by comparing them with simulations done in SPACAR[8][9]. SPACAR is a library in Matlab that uses beam theory to calculate the forces, moments, deformations and stresses in a flexure that consists of rectangular beams. Because the code of the SPACAR library can be altered, it is possible to adjust certain parameters or read out specific variables. Since the effects of shear have been neglected in the linear model, the effect of shear will also be turned off in the SPACAR code during this comparison.

3.2.1 Stiffness Matrix O-O

The stiffness matrix that couples the translation and rotation to the forces and moments of point O can be directly read out of SPACAR. In figures 8-10 each of the elements in the stiffness matrix is compared to the results from SPACAR. The elements are plotted against different variables that have an influence on the stiffness matrix seen in 78. These variables are the height (h), the length (L) and the width (w). Note that with this width, the influence of the moments of inertia in the stiffness matrix are verified. The following constants are used for these plots: $t = 0.001\text{m}$, $w = 0.05\text{m}$, $L = 0.15\text{m}$, $h = 0.4\text{m}$, $G = 70\text{GPa}$ and $E = 210\text{GPa}$

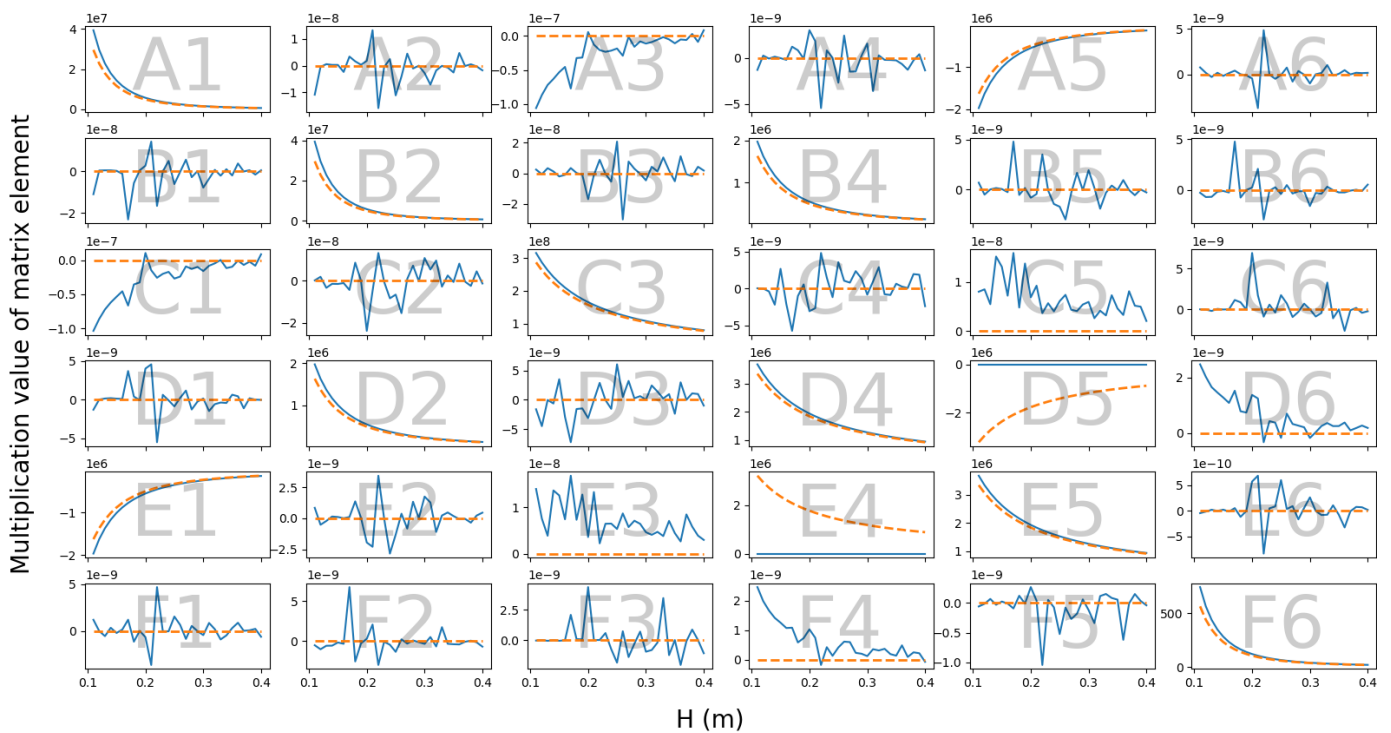


Figure 8: The values of each element of the stiffness matrix seen in equation 78 (dashed orange line) compared to the stiffness matrix results from SPACAR (blue line) plotted against the height (h).

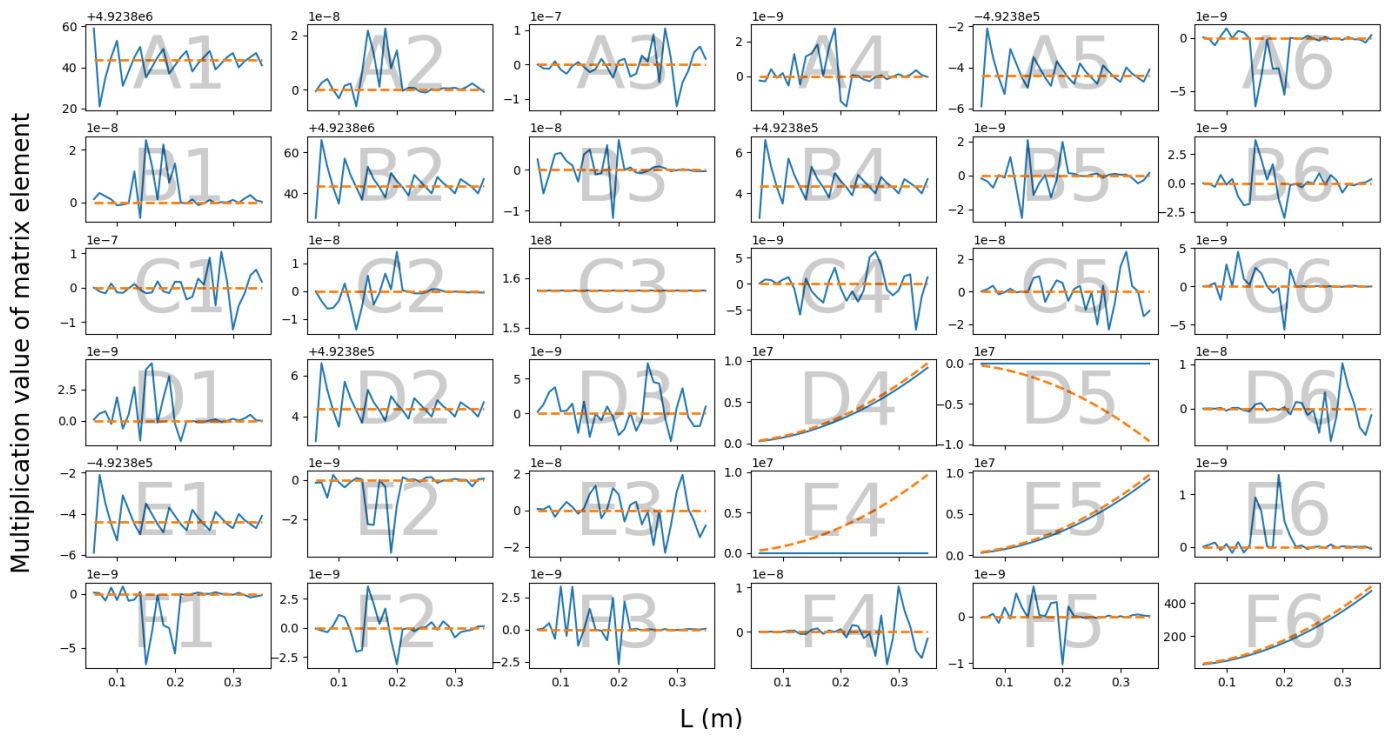


Figure 9: The values of each element of the stiffness matrix seen in equation 78 (dashed orange line) compared to the stiffness matrix results from SPACAR (blue line) plotted against the length (L).

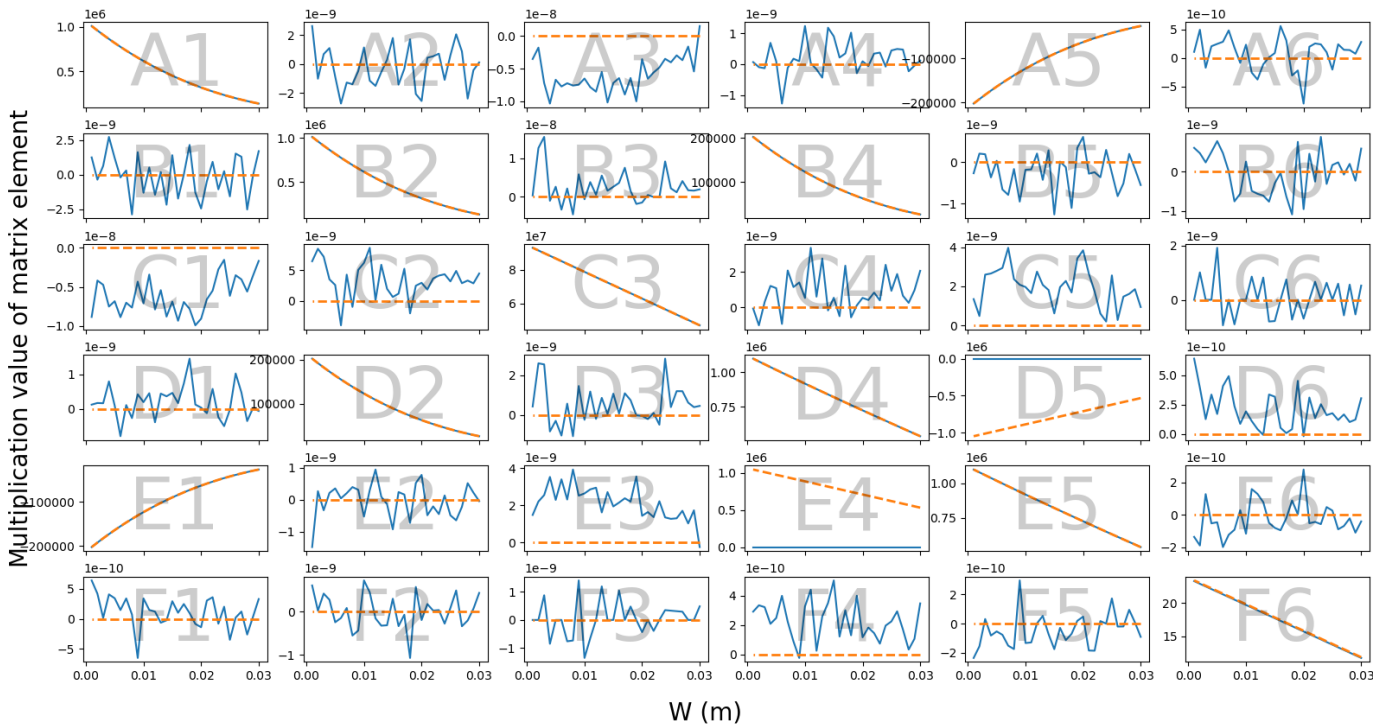


Figure 10: The values of each element of the stiffness matrix seen in equation 78 (dashed orange line) compared to the stiffness matrix results from SPACAR (blue line) plotted against the width (w).

One of the first things that is noticed when examining these figures is that the results from SPACAR seem to be unstable in most of the plots. This is caused due to the fact that the value for these elements is supposed to be zero. The small numeric inaccuracy in the SPACAR simulations, results in a numerical noise that is very close to zero. These results can be therefore be interpreted as

zero-values.

Further more, it can be seen that almost all elements of the derived stiffness matrix correspond with the results from SPACAR. Only element E4 and D5 seem to give varying results. Here SPACAR gives zero values while the derived stiffness matrix does not. This gives the impression that a small error has been made in the computation of this matrix. It can also be seen that due to element E4 and D5 the derived stiffness matrix is not symmetrical. According to Maxwell’s reciprocity theorem a stiffness matrix, that couples the displacements and rotations to the forces and moments of the same point, always has to be symmetrical [5]. This confirms the suspicion that a small error has been made. Luckily this error only influences the coupling of θ_x to M_y and θ_y to M_x . Since it has been derived that the input variables θ_x and θ_y can be approximated to zero, it is possible to continue and still use this stiffness matrix for the remainder of the report.

3.2.2 Stiffness Matrix O-tap

The stiffness matrix that couples the translation and rotation of point O to the forces and moments in the tapering cannot be directly read out of SPACAR. It is however possible to read out the forces in a constrained point. That is why to verify this stiffness matrix the forces and moments in point C will be calculated from the input displacement and rotation for different dimensions of the tapering. These results can then be compared to the data from SPACAR. The different dimensions of the leaf-springs that will

be used are: $\begin{pmatrix} w_1 & w_2 & w_3 \\ t_1 & t_2 & t_3 \end{pmatrix} = \begin{pmatrix} 0.05 & 0.05 & 0.05 \\ 0.001 & 0.001 & 0.001 \end{pmatrix} \text{m}$, $\begin{pmatrix} w_1 & w_2 & w_3 \\ t_1 & t_2 & t_3 \end{pmatrix} = \begin{pmatrix} 0.01 & 0.02 & 0.008 \\ 0.01 & 0.02 & 0.008 \end{pmatrix} \text{m}$
 and $\begin{pmatrix} w_1 & w_2 & w_3 \\ t_1 & t_2 & t_3 \end{pmatrix} = \begin{pmatrix} 0.01 & 0.02 & 0.008 \\ 0.01 & 0.02 & 0.008 \end{pmatrix} \text{m}$.

In the simulation in Matlab, the only degree of freedom that will be constrained is the input angle θ_z . All the other degrees of freedom will be unconstrained. The results of these simulations can be seen in figures 11-13.

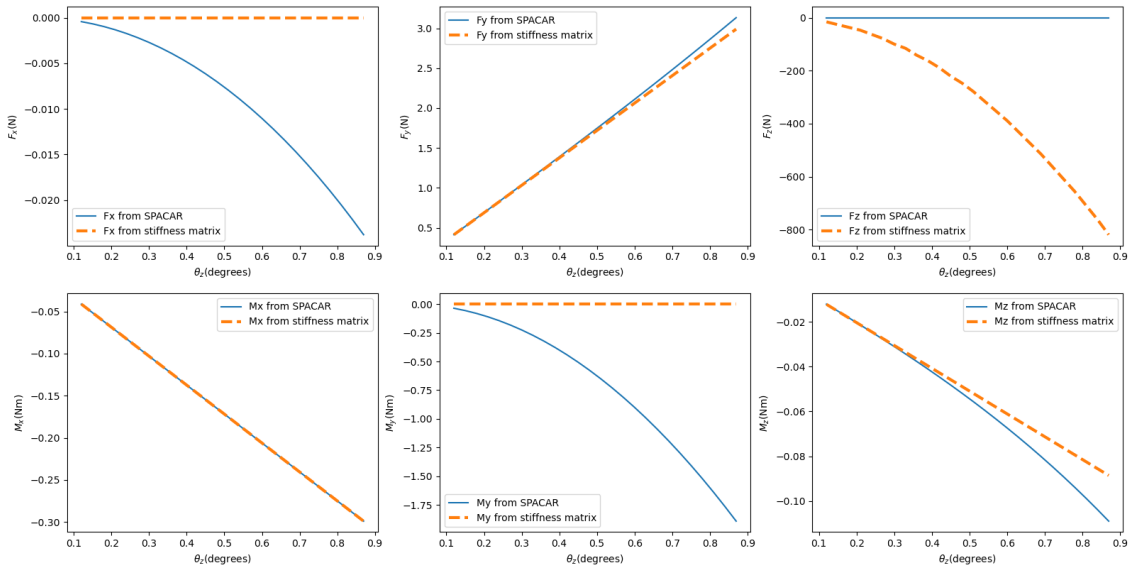


Figure 11: The forces and moments in point C derived from equation 80 (dashed orange line) and the forces and moments in point C computed by SPACAR (blue line) plotted against the input angle about the z-axis (θ_z). In this plot the following dimensions for the leaf-springs are used: $w_1 = w_2 = w_3 = 0.05\text{m}$ and $t_1 = t_2 = t_3 = 0.001\text{m}$.

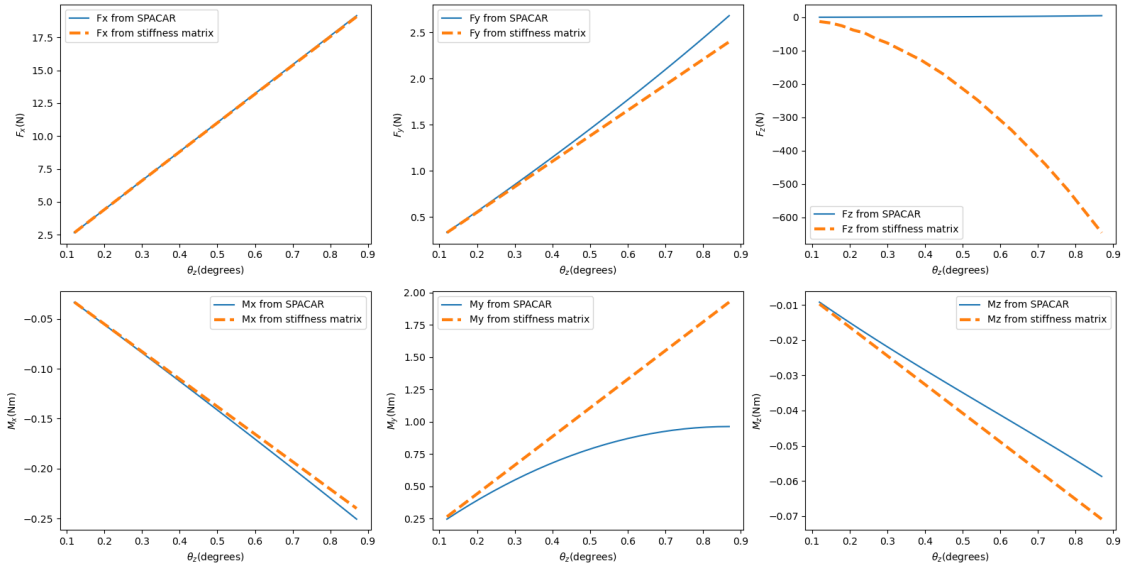


Figure 12: The forces and moments in point C derived from equation 80(dashed orange line) and the forces and moments in point C computed by SPACAR (blue line) plotted against the input angle about the z-axis (θ_z). In this plot the following dimensions for the leaf-springs are used: $w_1 = 0.04\text{m}$, $w_2 = 0.05\text{m}$, $w_3 = 0.06\text{m}$, $t_1 = 0.001$, $t_2 = 0.002$ and $t_3 = 0.0001\text{m}$.

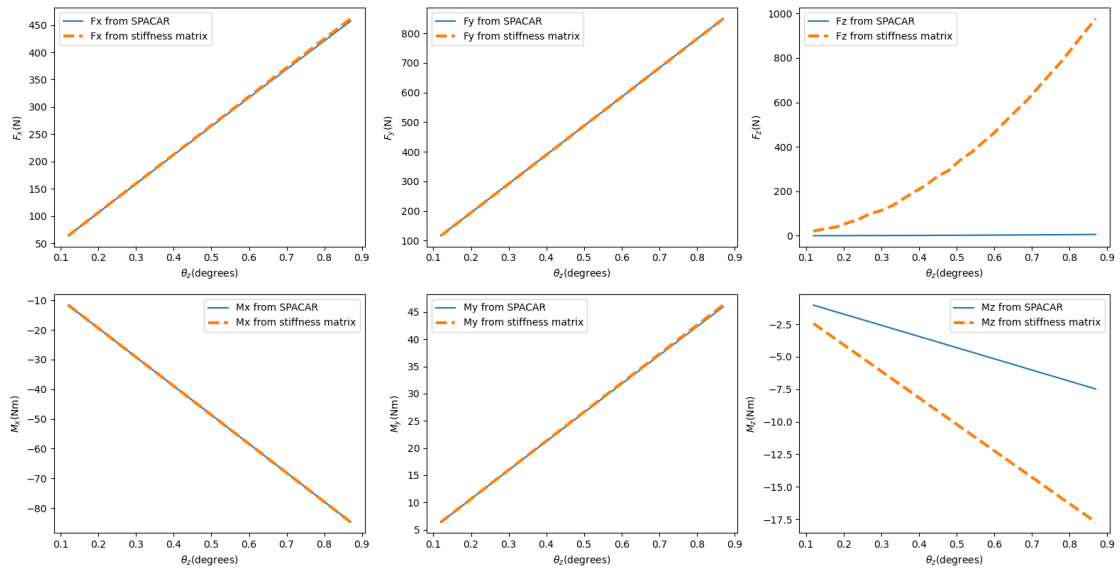


Figure 13: The forces and moments in point C derived from equation 80(dashed orange line) and the forces and moments in point C computed by SPACAR (blue line) plotted against the input angle about the z-axis (θ_z). In this plot the following dimensions for the leaf-springs are used: $w_1 = t_1 = 0.01\text{m}$, $w_2 = t_2 = 0.02\text{m}$ and $w_3 = t_3 = 0.008\text{m}$.

It can be said that the linear model gives the correct result when, for small deformations, the SPACAR results correspond to that of the model. In the figures it can be seen that this is the case for most of the results.

In other plots it can be seen that the stiffness matrix gives a zero value while SPACAR gives a non-zero value. It is assumed that

these non-zero values are caused by non-linear effects. This would mean that these differences do not indicate that the linear model is incorrect. They do however also not give any extra assurance that the linear model is correct.

Then finally, there are also some results which seem to be wrong at first glance. One of these results can be seen in the M_z against θ_z plot in figure 13. Here, it can be clearly seen that the lines have different slopes. This is caused due to the calculation of the torsional constant (eq. 63). In this equation it is assumed that the leaf-springs are thin walled. But, due to the fact that the cross-sectional area is squared in this case, the relation for the torsional constant is no longer valid. This explains the difference of the slope in the figure.

Then there is one relation left that seems to be inaccurate: In all of the figures above it can be seen in the determination of F_z that the linear model computes the force to be way higher than follows from SPACAR. This is caused by the height of the tapering being lowered a bit due to the bending and twisting of the beam. This is called shortening effect [1]. Because this effect lowers the height of the tapering, it also lowers the height of point O. Even though this deformation is small, it has a very big impact on calculating F_z in the linear model. This is due to the high factor of the element in the stiffness matrix corresponding to the relation between F_z and Δ_z .

From these results it can be concluded that the linear model gives a good representation of the forces and moments due to linear effects in the flexure, if the effects of shear can be neglected.

3.3 Stress determination from the linear model

In the previous sections the linear model has been determined and verified. From this model it is possible to derive the stresses within the leaf-springs of the flexure. These stresses are essential to determine at which turning angle the flexure mechanism will fail. In this section the stresses within the leaf-springs will be computed. From this a fail-criteria will be derived that describes when the tapering will start to deform plastically.

A common way to depict the stresses in an object is with a stress tensor[6]. A stress tensor is given by:

$$\sigma = \begin{pmatrix} \sigma_{xx} & \sigma_{xy} & \sigma_{xz} \\ \sigma_{yx} & \sigma_{yy} & \sigma_{yz} \\ \sigma_{zx} & \sigma_{zy} & \sigma_{zz} \end{pmatrix} = \begin{pmatrix} \sigma_{11} & \sigma_{12} & \sigma_{13} \\ \sigma_{21} & \sigma_{22} & \sigma_{23} \\ \sigma_{31} & \sigma_{32} & \sigma_{33} \end{pmatrix} \quad (81)$$

Here σ_{11} , σ_{22} and σ_{33} are the normal stresses. These stresses work in the perpendicular direction to their corresponding plane. σ_{12} , σ_{13} , σ_{21} , σ_{23} , σ_{31} and σ_{32} are the shear stresses. These shear stresses work in the parallel direction to that of their corresponding plane. A clearer view of the direction of the stresses can be seen in figure 14:

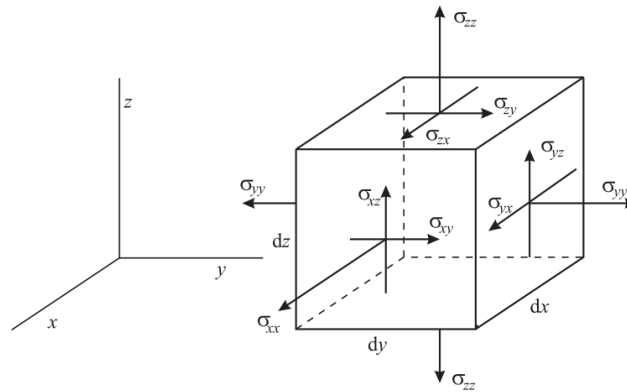


Figure 14: A schematic depiction of the direction of the components in the stress tensor.[3]

The stress in the flexure can be determined by calculating all the components of the stress tensor. One of the first things that can be done to derive these components, is to look at the simplification of the tensor. It is known that the stress tensor has to be symmetrical and thus $\sigma_{12} = \sigma_{21}$, $\sigma_{13} = \sigma_{31}$ and $\sigma_{23} = \sigma_{32}$ [3]. The matrix can be simplified further by looking at the approximations made earlier in section 3.1.2. For the derivation of the linear model, it is assumed that the leaf-springs deform according to Euler-Bernoulli beam theory. In this theory it states that the neutral line of a beam only moves in the transverse direction and that this transverse displacement is the same for all points in a cross-section. Because the neutral line is in the direction of the z -axis, it means that the normal stresses in the x - and y -direction and the shear stresses in the xy -plane are zero. The last approximation that will be made is that the shear stress in the yz -plane is negligibly small. This approximation can be made due to the fact that the stiffness in the y -direction is much smaller compared to the stiffness in the other directions. This also results in the stresses that act in the yz -plane to be a lot smaller and thus negligible[7].

The remaining stress components can be calculated directly from the forces, moments and deformations of the leaf-spring. To keep the stress equations as simple as possible, the origin of the x - and y -axis is translated such that it coincides with the centroid of cross-section in the leaf-spring. The equations that can be used to derive the stresses are:

The contribution of the forces to the normal stress can be calculated with[6]:

$$\sigma_{F_z} = \frac{F_{z,tap}}{A} \quad (82)$$

Here σ_{F_z} is the normal stress due to the contribution of the force in the z -direction.

The contribution of the moments to the normal stress is given by[6]:

$$\sigma_{M_x} = -y \frac{M_{x,tap}}{I_x} \quad (83)$$

$$\sigma_{M_y} = -x \frac{M_{y,tap}}{I_y} \quad (84)$$

Here σ_{M_x} and σ_{M_y} are the normal stresses due to the contribution of the corresponding moments.

The contribution of the forces to the shear stress is given by[6]:

$$\tau_{F_x} = -\frac{F_{x,tap}Q(x)}{I_y t} \quad (85)$$

$$\tau_{F_y} = \frac{F_{y,tap}Q(y)}{I_x w} \quad (86)$$

Here τ_{F_x} and τ_{F_y} are the shear stresses due to the contribution of the corresponding forces and $Q(x)$ and $Q(y)$ are the first moment of inertia given by:

$$Q(x) = \int x dA \text{ and } Q(y) = \int y dA \quad (87)$$

This first moment of area becomes zero due to the fact that the origin of the x - and y -axis coincide with the centroid of cross-section in the leaf-spring. This results in $\tau_{F_x} = \tau_{F_y} = 0$.

To determinate the contribution of the moments to the shear stress, the thin walled approximation described in [7] is used. The contribution to the shear stress is then given by:

$$\tau_{M_z} = -y \frac{M_{z,tap}}{I_x} \quad (88)$$

Here τ_{M_z} is the shear stress due to the contribution of the moment about the z -axis.

By combining these expressions, the remaining elements in the stress tensor can be determined. The stress tensor is then given by:

$$\sigma = \begin{pmatrix} 0 & 0 & G \frac{\partial \phi_z}{\partial z} 2y \\ 0 & 0 & 0 \\ G \frac{\partial \phi_z}{\partial z} 2y & 0 & \frac{F_{z,tap}}{A} - y \frac{M_{x,tap}}{I_x} - x \frac{M_{y,tap}}{I_y} \end{pmatrix} \quad (89)$$

The stresses within the leaf-springs have now been derived. The next step is to find a certain criteria which determines when the stress in a point is so big, that plastic deformation occurs. For this the equivalent stress, σ_{eq} , can be used. The equivalent stress is also known as the allowable stress and can help to describe when the stress has reached its critical value. This critical value depends on the criteria for the application of the flexure mechanism. In this case, the criteria is that there can be no plastic deformation in the flexure. In this case, the critical value is also known as the yield stress. Plastic deformation will occur when the equivalent stress becomes higher then this yield stress. The von Mises equivalent stress can be used for this criteria. This von Mises stress is widely used for the determination of the yield point of many engineering steels. The equivalent stress according to the von Mises criteria is given by [3]:

$$\sigma_{eq} = \sqrt{\frac{1}{2}((\sigma_{11} - \sigma_{22})^2 + (\sigma_{22} - \sigma_{33})^2 + (\sigma_{11} - \sigma_{33})^2 + 6(\sigma_{12} + \sigma_{13} + \sigma_{23}))} \quad (90)$$

Where σ_{eq} is the von Mises equivalent stress.

Substituting the components of the stress tensor into the equation gives us:

$$\sigma_{eq} = \sqrt{\left(\frac{F_{z,tap}}{A} - y \frac{M_{x,tap}}{I_x} - x \frac{M_{y,tap}}{I_y}\right)^2 + 3G \frac{\partial \phi_z}{\partial z} 2y} \quad (91)$$

The plastic deformation will start when this equivalent stress is higher than the yield stress. This critical stress is a mechanical property of the material in the flexure. The higher the yield stress, the more stress the flexure can endure before deforming plastically.

3.4 Verifying the stresses

In this section the stresses in the leaf-springs will be computed and compared to simulations in SPACAR. For these experiments the shear effects in SPACAR will be turned on again. This will give a better representation of the actual stress in the leaf-spring. From the comparisons between the results from SPACAR and the stresses derived from the linear model, it will be concluded when the linear model stops to be a valid representation for the stress in the leaf-springs.

By implementing the results of the linear model into equation 91, the linear contribution of the normal, shear and equivalent stress can be derived. The full expression of these stresses can be seen in appendix C. With the linear model it is derived that the flexure deforms by far the most in the direction about the z -axis. Because of this the terms with Δ_x , Δ_y , Δ_z , θ_x and θ_y are approximated to zero. This simplifies the stresses to:

$$\sigma_{33} = \frac{6E\theta_z Ly(h-2z)}{h^3} \quad (92)$$

$$\sigma_{13} = \sigma_{31} = \frac{2G\theta_z y}{h} \quad (93)$$

$$\sigma_{eq} = 2\sqrt{3}\sqrt{\frac{\theta_z^2 y^2 (3E^2 L^2 (h-2z)^2 + G^2 h^4)}{h^6}} \quad (94)$$

With the help of this equation the dimensions w , t , L and h can be chosen. From the equation for the equivalent stress, it can be seen that the stress compared to the height scales with the ratio $\sigma_{eq} \propto \frac{1}{h^2}$, that the stress scales linearly with the radius and thickness and that the stress is independent of the width.

From this it can be derived that for the dimensions of the leaf-springs, a relatively large height, low radius and low thickness is preferred. However increasing the height and decreasing the radius and thickness also decreases the stiffness of the entire flexure. This can cause the flexure to become unstable, which could make it lose its application value. An other important aspect to keep in mind has to do with is the fact that the leaf-spring does not revolve about its own center axis. Due to this, the part of the leaf-spring that is closest to the center of the flexure will deform less than a part that is further away. This is called the shortening effect. This effect has a big influence on the stress in the leaf-spring. Later in the report, the effect will be described in more detail¹.

To summarise: It is more favorable for the height to be higher and for the width, the thickness and the radius to be lower. These values can however not be too extreme, since this would result in the instability of the flexure or in the case of the length, a higher stress. Because of this, the dimensions chosen for this report are: $w = 0,03\text{m}$, $t = 0,001\text{m}$, $L = 0,1\text{m}$ and $h = 0,2\text{m}$.

For the computation of the stresses, the shear- and elasticity modulus also have to be chosen. For all upcoming simulations in this report the shear and elasticity modulus will be: $G = 77\text{GPa}$ and $E = 200\text{GPa}$. With this, the stresses in the leaf-springs can now be determined. These stresses can be seen in figure 15. To inspect the validity of the stresses they need to be compared to the simulation results from SPACAR. These results can be seen in figure 16.

By comparing figure 15 to figure 16abc, it can be seen that if the rotation angle is $\theta_z = \frac{1}{2}^\circ$, there are almost no differences between the stresses derived from the linear model and the stresses computed by SPACAR. From figure 16d it can be seen that the stress in the yz -plane is indeed very small. This confirms the assumption that this stress component is negligible. With these results it can be concluded that, for an angle of $\frac{1}{2}^\circ$, the stress derived from the linear model gives a good approximation for the real stress in the

¹More detail on the shortening effect can be seen in section sec:short

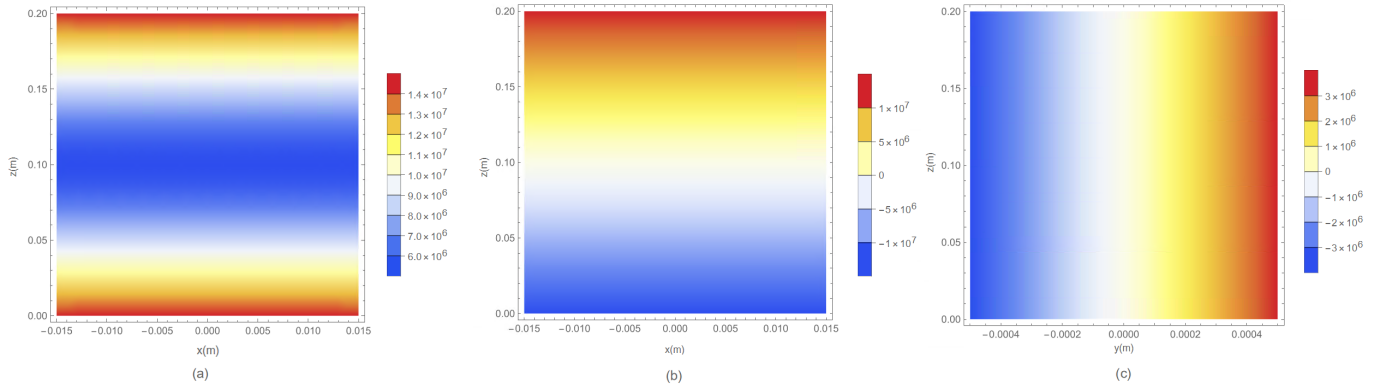


Figure 15: The stresses in the leaf-spring for an angle of $\theta_z = \frac{1}{2}^\circ$ derived from the linear model: (a) shows σ_{eq} in the xz -plane where $y = -\frac{T}{2}$, (b) shows σ_{33} in the xz -plane where $y = \frac{T}{2}$ and (c) shows σ_{13} in the yz -plane where $x = 0$.

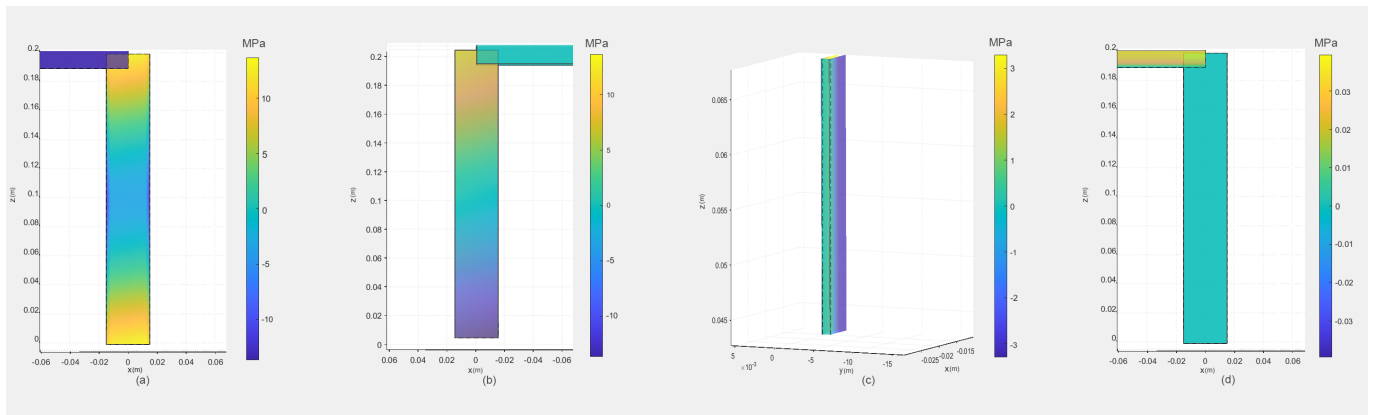


Figure 16: The stresses in the leaf-spring for an angle of $\theta_z = \frac{1}{2}^\circ$ computed in SPACAR, (a) shows σ_{eq} in the xz -plane where $y = -\frac{T}{2}$, (b) shows σ_{33} in the xz -plane where $y = \frac{T}{2}$, (c) shows σ_{13} in a 3D view and (d) shows σ_{13} where $y = -\frac{T}{2}$.

leaf-spring.

It is also interesting to inspect if this linear model will stay valid for larger angles. In figure 17, the equivalent stress for a rotation of $\theta_z = 2^\circ$ can be seen. In figure 17a the stress is derived from the linear model and in figure 17b the stress is computed by SPACAR. In these plots a clear difference emerges: The stress derived from the linear model seems to be independent of x while this is not the case for the stress computed by SPACAR. It can also be seen that the maximum equivalent stress is higher in the stress computation by SPACAR. These results show that the linear equivalent stress is no longer valid for a turning angle of $\theta_z = 2^\circ$. The differences between the plots are caused by non-linear effects. In the next chapter a closer look will be taken at these non-linear effects.

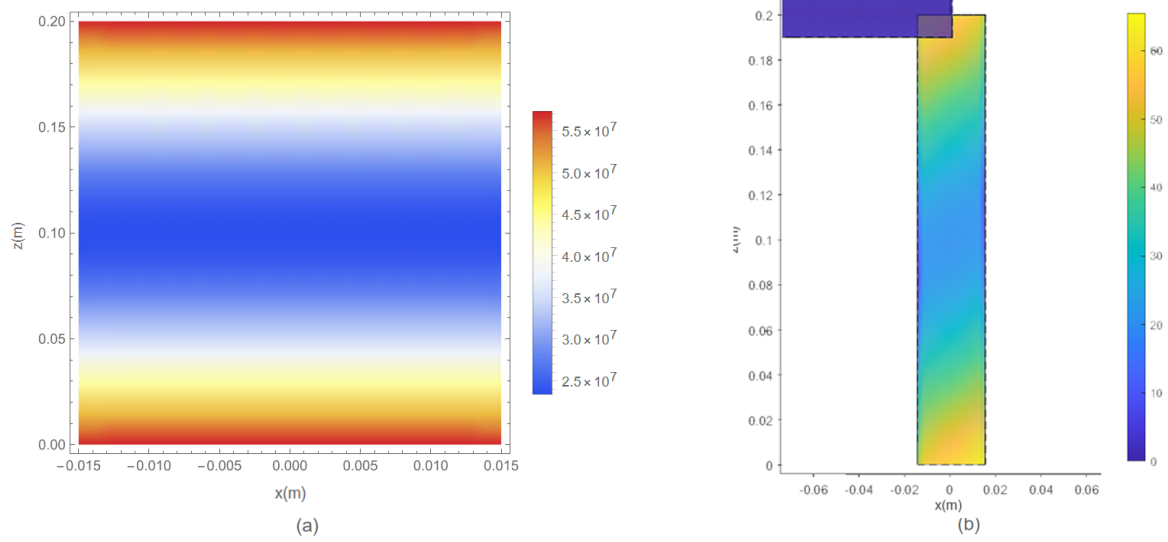


Figure 17: The equivalent stress in the leaf-spring for an angle of 2° , (a) shows the stress derived from the linear model and (b) shows the stress computed with SPACAR.

4 Non-linear Analysis

Up until this point in the report, the linear analysis of the leaf-springs has been discussed. In this analysis the stiffness matrices and the stress in the model have been derived. From this the direction of motion of the flexure and the dimensions of the leaf-spring have been determined. This linear model has been derived without taking into account the non-linear effects of the system. This results in the model losing its validity when the deformation in the flexure mechanism becomes to big.

This part takes a closer look at these non-linear effects. From the results, the shape of the tapering of the flexure will be derived. With this tapering it will be calculated how much the turning angle has increased.

4.1 The shortening effect

The non-linear effect that is investigated in this section is the shortening effect[10]. Figure 18 shows a leaf-spring when the flexure is rotated with the angle θ_z . It can be seen that the deformation of the leaf-springs increases with an increasing x . From section 3.1.7 it is known that the top of the leaf-springs does not rotate about the x - or y -axis. Because of this, the leaf-spring gets stretched in the z -direction. This stretching occurs primarily close to the top and bottom of the leaf-spring. This results in a high strain that is close to the top and bottom of the leaf-spring, which increases with the distance to the center of the flexure. This high strain also causes high stresses in these locations.

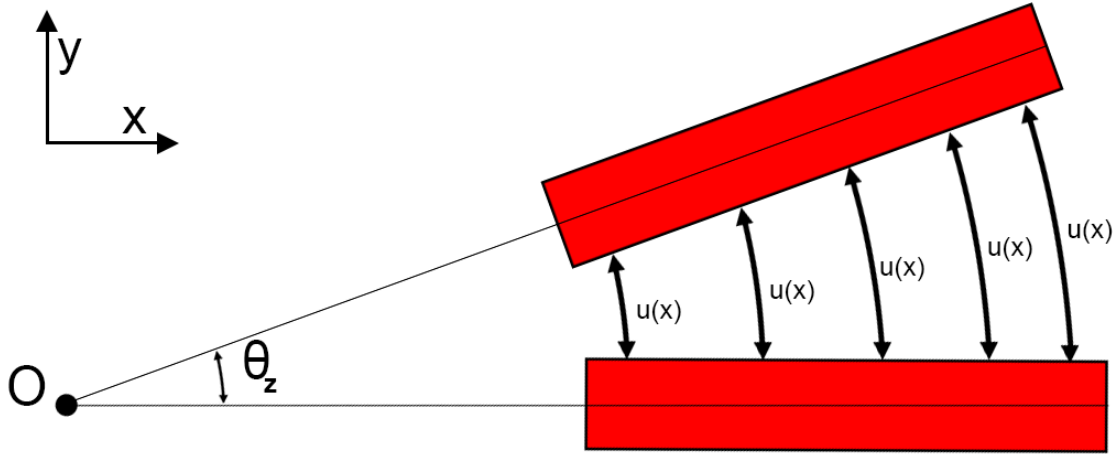


Figure 18: A leaf-spring when the flexure is rotated with the angle θ_z

The difference in deformation in the y -direction is significantly larger than the difference in deformation in the x -direction. Because of this, the shortening due to the deformation in the x -direction is neglected. The shortening due to the deformation in the y -direction can be calculated with [1]:

$$u_{z,shortening} \approx \frac{3}{5} \frac{u_y^2}{h} \quad (95)$$

where $u_{z,shortening}$ is the deformation in the z -direction due to the shortening.

By inserting the boundary condition for $u_y(z = h)$ (eq 67) into this equation, the total shortening of the leaf-spring can be calculated. In section 3.1.7, it is shown that Δ_y and θ_x can be approximated to zero. This results in the following equation for the shortening:

$$u_{z,totalshortening} \approx \frac{12}{5} \frac{(x \cos(\frac{\theta_z}{2}) \sin(\frac{\theta_z}{2}))^2}{h} \quad (96)$$

Here $u_{z,totalshortening}$ is the total shortening of the leaf-spring.

5 Designing the tapering

In this section a tapering is designed for the leaf-springs in the flexure. This is done by determining the ideal height-profile for the leaf-spring. A correctly chosen tapering decreases the maximum equivalent stress in the flexure and thus increases the possible turning angle.

For the least amount of stress due to shortening, it is best to keep the shortening constant throughout the leaf-spring. With this criteria a height profile can be derived from equation 96. This results in:

$$h_{short}(x) = \frac{12 (x \cos(\frac{\theta_z}{2}) \sin(\frac{\theta_z}{2}))^2}{5 C_{u_z, totalshortening}} \quad (97)$$

Where $h_{short}(x)$ is the ideal height profile of the leaf-spring to reduce the shortening effects and $C_{u_z, totalshortening}$ is a constant.

It is known that the height of the leaf-spring has to be maximal when $x = L$. With this the equation can be rewritten as:

$$h_{short}(x) = \frac{h_{max}x^2}{L^2} \quad (98)$$

where h_{end} is the height of the not tapered leaf-spring.

It is also important to keep the stress due to the linear effects in mind. In section 3.4, it is derived that the linear equivalent stress scales with the height according to the ratio: $\sigma_{eq,lin} \propto \frac{1}{h^2}$. Since the tapering of the leaf-springs lowers the height, it also increases the linear equivalent stress. Because of this, it is important to find the optimal balance between reducing the effects of shortage and making sure that the linear stress will not become too high. To find this optimal balance, the height profile in equation 98 will be multiplied with a factor to decrease the height of the tapering. This results in the following equation for the height profile of the leaf-spring:

$$h_{tapering}(x) = \gamma \frac{h_{end}x^2}{L^2} \quad (99)$$

Where $h_{combined}(x)$ is the height profile of the leaf-spring and γ is a multiplication factor between 0 and 1.

Before this multiplication factor can be determined, it is important to determine what type of tapering is used for the flexure. The two cases that will be inspected in this report are depicted in figure 19. In the first case (figure 19a), the leaf-spring is only tapered on one side. In the second case (figure 19b), the leaf-spring is tapered on both sides. Here each of the sides contribute half of the total desired tapering. This second type of tapering is inspired by [2]. To prevent stress localisation[11], the edges between the leaf-spring and the tapering are rounded with a filet with a radius of 1 mm.

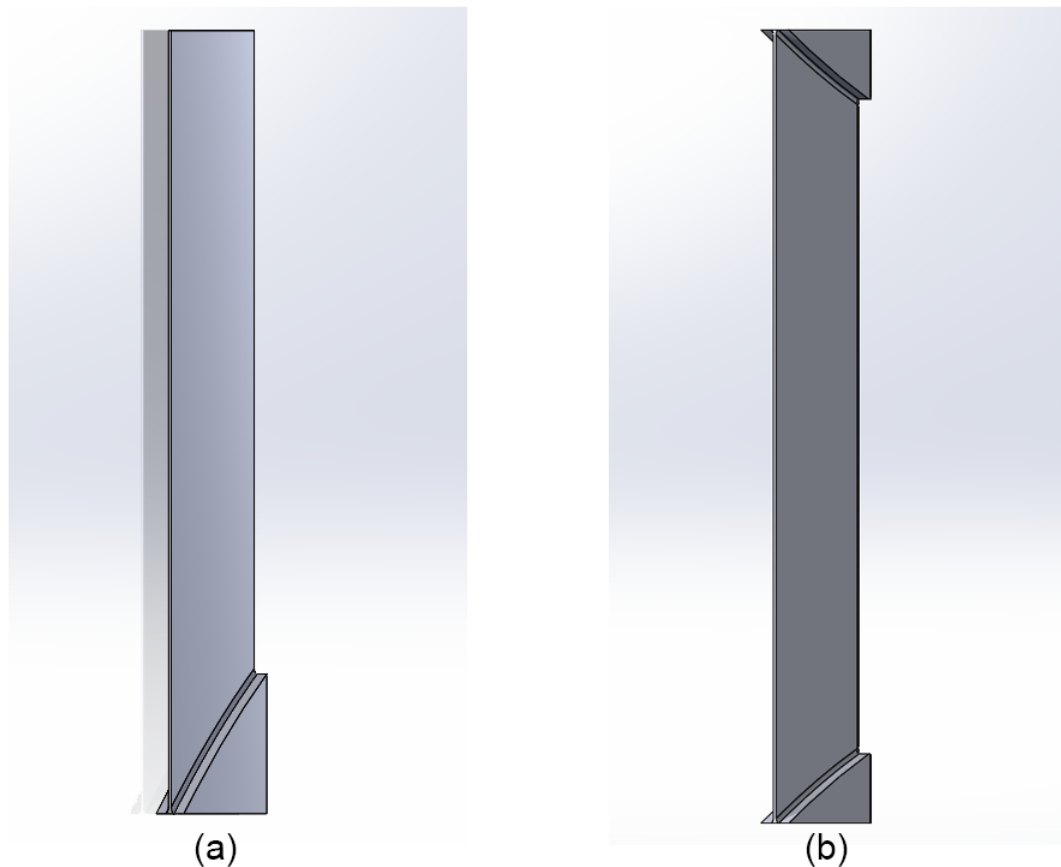


Figure 19: The two types of possible tapering. (a) shows the leaf-spring only being tapered on one side and (b) shows the leaf-spring being tapered from both sides.

It is important to note that the ideal multiplication is dependent on θ_z . From equation 94 it can be seen that the linear equivalent stress scales linearly with the angle about the z -axis. However in equation 98 it can be seen that the shortening scales approximately quadratic with the this same angle. This means that the effects of the shortening has more influence on the total stress for larger angles about the z -axis. This results in the increase of the multiplication factor for an increasing angle of rotation about the z -axis.

The shortening effect acts close to both the top and bottom of the leaf-spring. This causes the effect to be cancelled out more when the leaf-spring is tapered from both the top and bottom. Because of this, it is also expected that the tapering of both sides results in a lower maximum stress.

To verify this, a simulation is done to check which type of tapering has the highest equivalent stress when both are turned with the same angle. For this simulation ANSYS Mechanical is used. ANSYS Mechanical is a finite element simulation program that can be used to analyse the behaviour of structures. The material in ANSYS that is chosen for this and all other simulation in the report is structural steel. This material has the same elasticity and shear modules as in the report. In section 3.1.7, it has been derived what the deformation in the flexure mechanism will be. Because of this, it is know what the deformation on the top and bottom of one specific leaf-spring is. With this, it is possible to simulate only one leaf-spring instead of the entire flexure. This greatly reduces the computation time of a simulation.

The results of the simulations, where the leaf-springs are rotated with an angle of $\theta_z = 0.35^\circ$, can be seen in figure 20.

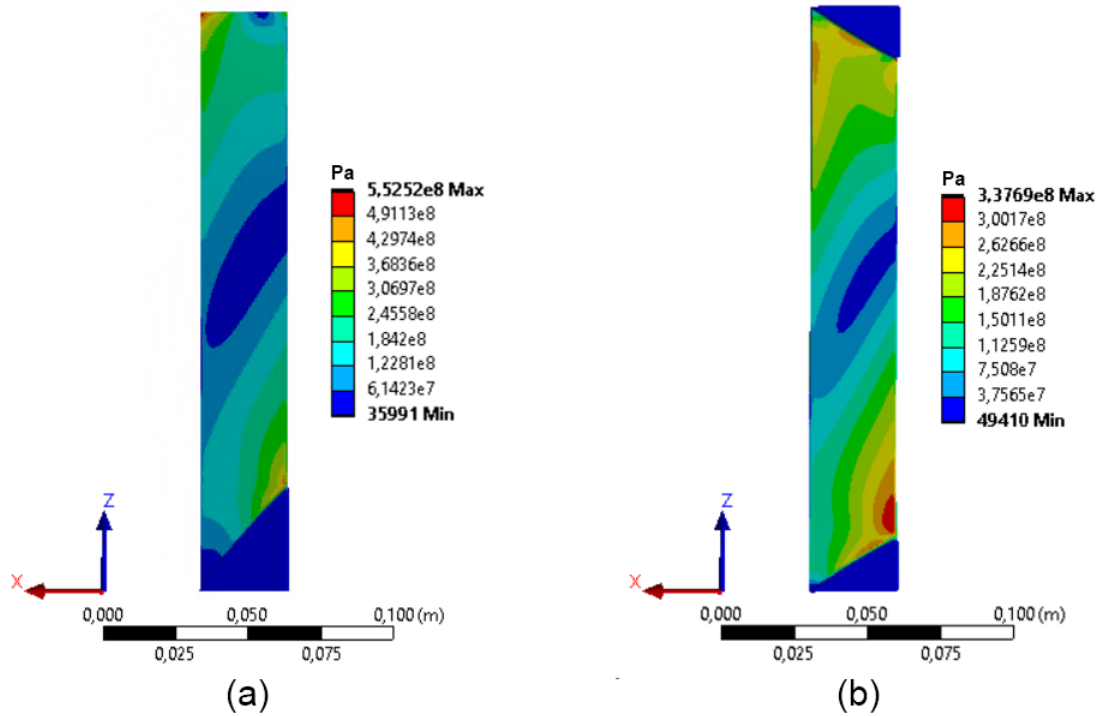


Figure 20: The equivalent stress in the two types of tapering when they are turned with an angle of $\theta_z = 0.35^\circ$. (a) shows the leaf-spring that is only tapered on one side and (b) shows the leaf-spring that is tapered from both sides.

From figure 20a it can be seen that the maximum stress is highly concentrated in the tip of the corner when the leaf-spring is tapered on one side. This is the result that is expected from the stress due to the shortening effect. In figure 20b it can be seen that the maximum stress is distributed much more evenly when both sides are tapered. This maximum stress is also not as high as in the first case. From these observations it can be concluded that the tapering of the leaf-spring on both sides is the better type of tapering.

5.1 Determining the multiplication factor

All the necessary information has now been acquired to start to compute the ideal multiplication factor. This will be done by running simulations in ANSYS for various multiplication factors. From each of these simulations the maximum equivalent stress will be determined. All of these stresses will then be plotted against their multiplication factor. The result of this can be seen in figure 21.

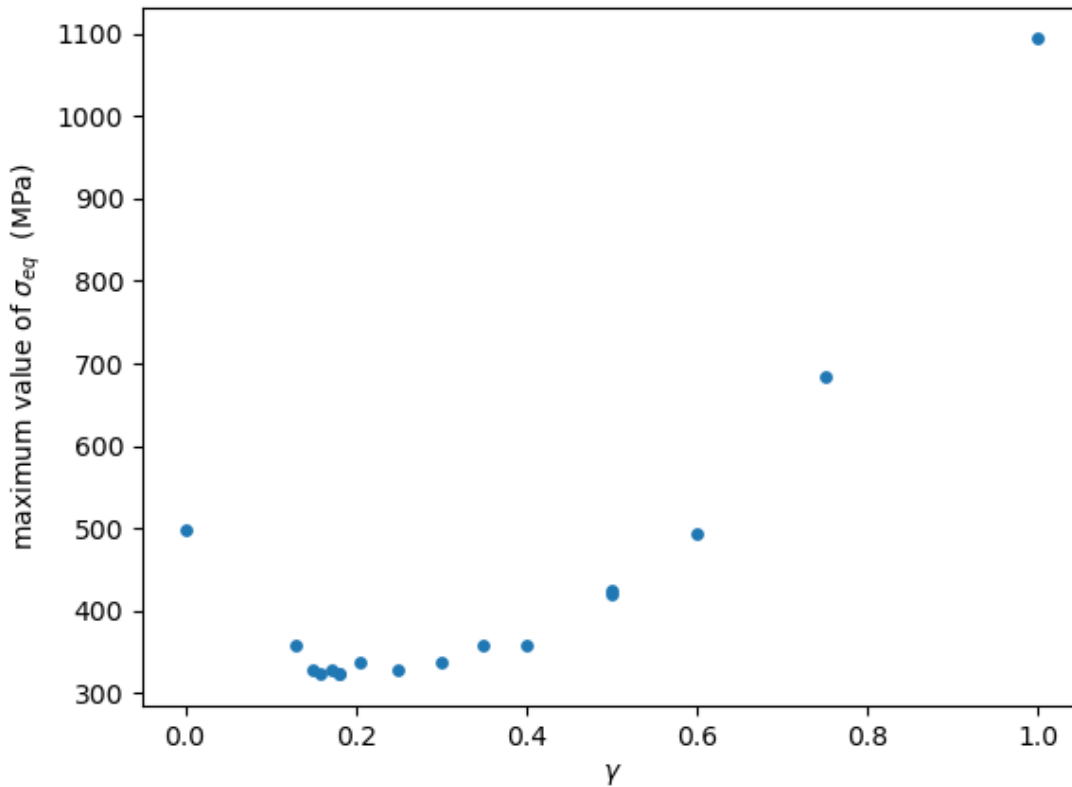


Figure 21: Simulation results of the maximum equivalent stress in the leaf-spring, σ_{eq} , plotted against the multiplication factor, γ , when the flexure is turned with an angle of $\theta_z = 7^\circ$.

From this figure it can be seen that the maximum equivalent stress decreases until it reaches its minimal value around $\gamma = 0.18$ after which it starts to increase. This corresponds with our expectation that for a low multiplication factor the shortening effect has a lot of influence on the maximum equivalent stress, while for higher multiplication factors this influence decreases. It can then also be seen that when the multiplication factor becomes higher, other stresses increase the maximum equivalent stress.

The maximum equivalent stress reaches its minimal value when the multiplication factor is around $\gamma = 0.18$. This means that the ideal multiplication value for an angle of $\theta_z = 7^\circ$ is approximately 0.18.

6 Calculating the maximum turning angle

With the now determined multiplication factor, the maximum turning angle for this multiplication factor can be computed. This can be done by varying the turning angle for different simulations until the maximum equivalent stress in the system is just below the yield stress. This angle is then the maximum turning angle for that specific multiplication factor. From ANSYS it can be seen that the yield stress of the material "structural steel" is 250MPa. As earlier derived, the multiplication factor that will be used is 0.18. With this the maximum angle can be determined for the flexure with and without the tapering.

For the leaf-springs where no tapering is applied, the maximum turning angle of the system is $\theta_{z,max} = 4.8^\circ$. For the leaf-springs where the derived tapering is applied, the maximum turning angle of the system is $\theta_{z,max} = 6^\circ$. This means that the tapering has increased the turning angle with 25%. With this new turning angle the tapering has a turning range of 12° .

It is important to mention that no safety factors have been taken into account for this turning range. It is therefore recommended for application purposes to, decrease the maximum turning angle with a safety factor. This safety factor can be determined by performing an error analysis.

7 Conclusion

In this report, a tapering has been designed for a radially oriented flexure joint to increase the maximum turning angle. An increased maximum turning angle will also increase the application possibilities of the flexure mechanism. An application for this flexure, could for example be a bearing that cancels out the effect of the rotation of the earth for the METIS instruments in the Extremely Large Telescope.

The maximum turning angle has been increased by redesigning the tapering of the flexure. To do this, a linear model has been derived that can describe forces, moments and stresses in the flexure as a function of the displacement and rotation. This model shows that the flexure mechanism is well behaved and almost only deforms by rotating about its z-axis. The dimensions of the leaf-spring have also been determined with the help of this model. From the stresses in the model it has been derived that the equivalent stress resulting from the linear effects in the system is given by equation 94.

It has also been determined that the non-linear shortening effect has a significant influence on the stresses in the flexure. By taking this shortening effect and the linear effects into account, the most optimal tapering has been derived. From this, it follows that leaf-springs have to be tapered according to the height profile in equation 99. In this equation the ideal multiplication factor depends on the turning angle of the flexure. For the best performance, this turning angle has to be equal to the maximum turning angle of the flexure. When the turning angle is 7 degrees, which is an original approximation for the maximum turning angle of the flexure, the ideal multiplication factor is 0.18.

The tapering that can be designed with this multiplication factor increases the maximum turning angle of the radially oriented flexure joint from 4.8 to 6 degrees.

8 Discussion

During this research a lot of results have been derived and discussed. The most noteworthy of these, together with some remarks, will be discussed in the following.

First of all in this report a lot of effects have been neglected. These effects include the shear due to deformation, the approximations made in the Bernoulli Euler beam theory and all non-linear effects apart from the shortage due to the deformation in the y -direction. Although these approximations have proven to be valid for this case, they might not be valid when the dimensions of the leaf-springs are changed. If for example the width of the leaf-springs is increased, then it is possible that the shear effects become so large that they cannot be neglected any more. This is important to take this into account when designing the tapering in a flexure using the theory described in this report.

Furthermore it is also worth to mention that the scope of this report has been to derive the ideal shape of the tapering. This tapering then increases the maximum turning angle of the flexure. Other improvements, as for example a different material or other dimensions for the leaf-spring, have not been researched. When designing a radially oriented flexure mechanism, it is recommended to also look into the effect these changes have on the properties of the flexure.

An other interesting remark is, that the approach taken to determine the height profile of the leaf-spring can also partly be seen in [2]. Here the type of tapering is described together with the same correlation between the height and stress and between the height and radius of the leaf-spring. This helps to confirm that the approach taken in this report is correct.

An issue can be seen while comparing the stiffness matrix in equation 78 with the results from the SPACAR simulations. It can be seen that element E4 and D5 of this stiffness matrix do not correspond with the results from SPACAR. From this it seems like an error has been made deriving these components of the stiffness matrix. Also, it is known from [5] that a stiffness matrix has to be symmetrical. Since this is not the case due to element E4 and D5, it confirms that an error has indeed been made deriving the stiffness matrix. However, in that same section and in the analytical analysis in Appendix B it is derived that when only a force in and a moment about the z -direction is applied to the system, that then the rotation about the x - and y -axes is zero. This means that, in the application of our flexure, elements E4 and D5 are multiplied by zero. Because of this, the stiffness matrix can still be used in the rest of the report.

The final point that will be discussed is the determination of the multiplication factor γ . From the report, it is known that this factor is dependent on the angle about the z -axis. To get the best result, the simulations to determine the multiplication factor has to be done with the maximum turning angle of the system. However, this maximum turning angle is not known before hand. This means that to get the best multiplication factor, the simulations have to be done over and over again until the angle used in the simulations is in fact the maximum turning angle of the system. In the report the simulations have only been done for one turning angle. The angle used for this turned out to be bigger then the maximum turning angle. The tapering in the flexure can thus be improved further by choosing an angle for the simulations that is closer to the maximum turning angle of the flexure mechanism.

9 Plagiarism check

On this paper, a plagiarism scan is performed. This is demanded by the Applied Physics education. The overall similarity value between other documents is 8%. This overlap only consist of the references, parts of equations or general parts of a sentence, e.g. "that the equivalent stress resulting from this is". From this it can be concluded that no plagiarism has been committed in this report.

10 Acknowledgement

I would like to thank Marijn Nijenhuis for his guidance and assistance during this study. During our meetings, Marijn has taught me a lot about precision engineering and we had interesting conversations about the data and next steps in the research. Furthermore, with his kind personality Marijn made me feel welcome in the Precision Engineering group.

I also want to thank Hans Kanger for his help and for taking the time to be part of my bachelor committee.

I want to thank Axel Lok for giving my access to the server on which I could run my simulations.

I also want to thank Carlijn van Emmerik for her help preparing for my bachelor assignment.

Finally, I would like to thank the complete Precision Engineering group for enabling me to go through this extremely educational experience.

References

- [1] M. Nijenhuis, J. Meijaard, and D. Brouwer, “A spatial closed-form nonlinear stiffness model for sheet flexures based on a mixed variational principle including third-order effects,” August 2020.
- [2] L. Hale, “Principles and techniques for designing precision machines,” Februari 1999.
- [3] H. Tjerdeman and R. M. E. J. Spiering, “Solid mechanics 1, elasticity,” January 2005.
- [4] B. R. Brandl, R. Lenzen, E. Pantin, A. Glasse, J. Blommaert, L. Venema, F. Molster, R. Siebenmorgen, S. Kendrew, M. Baes, H. Böhnhardt, W. Brandner, E. van Dishoeck, T. Henning, H. U. Käußl, P.-O. Lagage, T. J. T. Moore, C. Waelkens, and P. van der Werf, “Instrument concept and science case for the mid-ir e-elt imager and spectrograph metis.”
- [5] H. P. Gavin, “Mathematical properties of stiffness matrices,” May 13 2014.
- [6] B. M. de Gooijer and J. P. Schilder, “Mechanics of material,” September 2021.
- [7] N. Trahair, “Flexural-torsional buckling of structures,” 1993.
- [8] J. B. Jonker and J. P. Meijaard, “Spacar- computer program for dynamic analysis of flexible spatial mechanisms and manipulators,” in *Multibody Systems Handbook*, W. Schiehlen, Ed. Berlin: Springer, 1999, pp. 123–143.
- [9] ———, “A geometrically non-linear formulation of a three dimensional beam element for solving large deflection multibody system problems.” in *International Journal of Non-Linear Mechanics*, July 2013, pp. 63–74.
- [10] S. Awtar, A. Slocum, and E. Sevincer, “Characteristics of beam-based flexure modules,” in *Journal of mechanical design*.
- [11] F. Hélénon, M. Wisnom, S. Hallett, and G. Allegri, “An approach for dealing with high local stresses in finite element analyses,” in *Composites Part A: Applied Science and Manufacturing, Volume 41, Issue 9*, 2010, pp. 1156–1163.

Appendix

A Analytical calculation of the linear model

In this chapter part of the solution for the linear model is derived analytically. In section 3.1 the Equilibrium equations, the displacement of point A/B and C and the stiffness equations are determined. With this, the deformation of the flexible beam can be derived. In this section the deformation will be derived for 2 cases: if there is no F_z component present and when there is an F_z component present in the beam.

To compress the size of the equations, the forces and moments of the flexible beam have been indicated with the subscript 2. So this means that:

$$F_{x,rigid} = F_{x2} \quad (100)$$

$$F_{y,rigid} = F_{y2} \quad (101)$$

$$F_{z,rigid} = F_{z2} \quad (102)$$

$$M_{x,rigid} = M_{x2} \quad (103)$$

$$M_{y,rigid} = M_{y2} \quad (104)$$

$$M_{z,rigid} = M_{z2} \quad (105)$$

$$(106)$$

For the same reason, the derivatives in this appendix will be denoted with an apostrophe.

With this, and with the equations seen in section 3.1, the linear analysis can be done.

A.1 Determining of the deformation if $F_z = 0$

First the deformation in the x-direction will be derived, then the deformation in the y-direction and then the turning angle in the z-direction.

A.1.1 Deformation in the x-direction

From the following stiffness and equilibrium-equations for the deformation in the x-direction:

$$M_{1,y,2}(z) = EI_y \kappa_{y1} = -EI_y u''_{1x} \quad (107)$$

$$M_{1,y,2} = -M_{y,B} + (h_1 - z)F_{1,x,2} + u_{1,x}F_{1,z,2}u'_{1,x} \quad (108)$$

it can be derived that

$$u_{1,x}(z) = \int \int \left(\frac{1}{EI_y} M_{y,B} - (h_1 - z)F_{1,x,2} - u_{1,x}F_{1,z,2} \right) dz^2 \quad (109)$$

where $h_1 = h - \Delta h$.

By applying the boundary conditions:

$$u'_{1,x}(z=0) = -\phi_{y1}(z=0) = 0 \quad (110)$$

$$u'_{1,x}(z=h_1) = -\phi_{y1}(z=0) = -\theta_y \quad (111)$$

$$u_{1,x}(z=0) = 0 \quad (112)$$

$$u_{1,x}(z=h_1) = \Delta x - 2L \sin\left(\frac{\theta_z}{2}\right) \sin\left(\frac{\theta_z}{2}\right) + L(\cos(\theta_y) - 1) \quad (113)$$

It can be derived that:

$$u_{1x}(z) = -\frac{1}{EI_{y1}} \left((h_1 \frac{1}{4} z^2 - \frac{1}{6} z^3) F_{1x,2} + \int \int u_{1x}(z) F_{1z,2} ds - \frac{1}{2h_1} z^2 \int u_{1x}(h_1) F_{1z,2} ds + \frac{1}{2h_1} z^2 EI_{y1} \theta_y \right) \quad (114)$$

$$u_{1x}(h_1) = -\frac{1}{EI_{y1}} \left(\frac{1}{12} h_1^3 F_{1x,2} + \frac{1}{2} h_1 EI_{y1} \theta_y + \int \int u_{1x}(h_1) F_{1z,2} ds^2 - \frac{1}{2} h_1 \int u_{1x}(h_1) F_{1z,2} ds \right) = \Delta x - 2L \sin\left(\frac{\theta_z}{2}\right) \sin\left(\frac{\theta_z}{2}\right) + L(\cos(\theta_y) - 1) \quad (115)$$

A.1.2 Deformation in the y-direction

From the following stiffness and equilibrium-equations for the deformation in the y-direction:

$$M_{x1}(z) = EI_x \kappa_{x1} = EI_x u''_{1y} \quad (116)$$

$$M_{1x,2} = -M_{x,B} - (h_1 - z) F_{1y,2} - u_{1y}(z) F_{1z,2} \quad (117)$$

$$(118)$$

It can be derived that:

$$u_{1y}(z) = \frac{1}{EI_x} \int \int (-M_{x,B} - (h_1 - z) F_{1y,2} - f_y(z) F_{1z,2}) dz^2 \quad (119)$$

By applying the boundary conditions:

$$u'_{1y}(z=0) = \phi_{x1}(z=0) = 0 \quad (120)$$

$$u'_{1y}(z=h_1) = \phi_{x1}(z=h_1) = \theta_y \quad (121)$$

$$u_{1y}(z=0) = 0 \quad (122)$$

$$u_{1y}(z=h_1) = \Delta y - 2L \sin\left(\frac{\theta_z}{2}\right) \cos\left(\frac{\theta_z}{2}\right) + L(\cos(\theta_x) - 1) \quad (123)$$

It can be derived that

$$u_{1y}(z) = \frac{1}{EI_{x1}} \left(-(h_1 \frac{1}{4} z^2 - \frac{1}{6} z^3) F_{1y,2} - \int \int u_{1y}(z) F_{1z,2} ds^2 + \frac{1}{2h_1} z^2 \int u_{1y}(h_1) F_{1z,2} ds + \frac{1}{2h_1} z^2 EI_{x1} \theta_x \right) \quad (124)$$

$$(125)$$

$$u_{1y}(h_1) = \frac{1}{EI_{x1}} \left(-\frac{1}{12} h_1^3 F_{1y,2} + \frac{1}{2} h_1^2 EI_{x1} \theta_x - \int \int u_{1y}(h_1) F_{1z,2} ds^2 + \frac{1}{2} h_1 \int u_{1y}(h_1) F_{1z,2} ds \right) = \Delta y - 2L \sin\left(\frac{\theta_z}{2}\right) \cos\left(\frac{\theta_z}{2}\right) + L(\cos(\theta_x) - 1) \quad (126)$$

A.2 Turning angle

From the following stiffness and equilibrium-equations for the turning angle in the z-direction:

$$M_{1z,2}(z) = GJ_1 \kappa_{z1} = GJ_1 \phi'_{z1} \quad (127)$$

$$M_{1z,2} = -M_{z,B} + u_{1y}(z) F_{1x,2} - u_{1x}(z) F_{1y,2} \quad (128)$$

$$M_{z,B} = M_{z,O} + LF_{1y,2} \quad (129)$$

it can be derived that:

$$\phi_{z1} = \frac{1}{GJ_1} \left(-(M_{z,O} + LF_{1y,2})z + \int (u_{1y}(z) F_{1x,2} - u_{1x}(z) F_{1y,2}) ds \right) \quad (130)$$

By applying the boundary condition:

$$\phi_{z1}(z=h_1) = \theta_z \quad (131)$$

it can be derived that:

$$\phi_{z1}(h_1) = \frac{1}{GJ_1} \left(-(M_{z,O} + LF_{1y,2})h_1 + \int (u_{1y}(h_1) F_{1x,2} - u_{1x}(h_1) F_{1y,2}) ds \right) = \theta_z \quad (132)$$

A.3 Rotation of the axis

With equation 100-132, the formula's for deformation are derived for the flexible beam 1. For flexible beam 2 and 3 these calculations don't have to be done again. The axis of the forces, moments and displacements calculated for beam 1, can be simply rotated to derive the equations for beam 2 and 3. The rotation used for this is depicted in figure 7.

The corresponding rotation matrices are:

$$\begin{pmatrix} x'_2 \\ y'_2 \end{pmatrix} = \begin{pmatrix} \cos(\alpha) & \sin(\alpha) \\ -\sin(\alpha) & \cos(\alpha) \end{pmatrix} \begin{pmatrix} x \\ y \end{pmatrix} = \begin{pmatrix} -\frac{1}{2} & \frac{\sqrt{3}}{2} \\ -\frac{\sqrt{3}}{2} & -\frac{1}{2} \end{pmatrix} \begin{pmatrix} x \\ y \end{pmatrix} \quad (133)$$

$$\begin{pmatrix} x'_3 \\ y'_3 \end{pmatrix} = \begin{pmatrix} \cos(2\alpha) & \sin(2\alpha) \\ -\sin(2\alpha) & \cos(2\alpha) \end{pmatrix} \begin{pmatrix} x \\ y \end{pmatrix} = \begin{pmatrix} -\frac{1}{2} & -\frac{\sqrt{3}}{2} \\ \frac{\sqrt{3}}{2} & -\frac{1}{2} \end{pmatrix} \begin{pmatrix} x \\ y \end{pmatrix} \quad (134)$$

$$\begin{pmatrix} x \\ y \end{pmatrix} = \begin{pmatrix} \cos(2\alpha) & \sin(2\alpha) \\ -\sin(2\alpha) & \cos(2\alpha) \end{pmatrix} \begin{pmatrix} x'_2 \\ y'_2 \end{pmatrix} = \begin{pmatrix} -\frac{1}{2} & -\frac{\sqrt{3}}{2} \\ \frac{\sqrt{3}}{2} & -\frac{1}{2} \end{pmatrix} \begin{pmatrix} x \\ y \end{pmatrix} \quad (135)$$

$$\begin{pmatrix} x \\ y \end{pmatrix} = \begin{pmatrix} \cos(\alpha) & \sin(\alpha) \\ -\sin(\alpha) & \cos(\alpha) \end{pmatrix} \begin{pmatrix} x'_3 \\ y'_3 \end{pmatrix} = \begin{pmatrix} -\frac{1}{2} & \frac{\sqrt{3}}{2} \\ -\frac{\sqrt{3}}{2} & -\frac{1}{2} \end{pmatrix} \begin{pmatrix} x \\ y \end{pmatrix} \quad (136)$$

$$(137)$$

Note that the apostrophe here indicates the changed axis, it does not indicate a derivative.

Our new coupling equations in point O then become:

$$0 = F_{1,x,o} + F_{2,x,o} + F_{3,x,o} \quad (138)$$

$$0 = F_{1,x,o} - \frac{1}{2}F_{2,x'_2,o} + \frac{\sqrt{3}}{2}F_{2,y'_2,o} - \frac{1}{2}F_{3,x'_3,o} - \frac{\sqrt{3}}{2}F_{3,y'_3,o} \quad (139)$$

$$0 = F_{1,y,o} + F_{2,y,o} + F_{3,y,o} \quad (140)$$

$$0 = F_{1,y,o} - \frac{\sqrt{3}}{2}F_{2,x'_2,o} - \frac{1}{2}F_{2,y'_2,o} + \frac{\sqrt{3}}{2}F_{3,x'_3,o} - \frac{1}{2}F_{3,y'_3,o} \quad (141)$$

$$0 = F_{1,z,o} + F_{2,z,o} + F_{3,z,o} \quad (142)$$

$$0 = M_{1,x,o} + M_{2,x,o} + M_{3,x,o} \quad (143)$$

$$0 = M_{1,x,o} - \frac{1}{2}M_{2,x'_2,o} + \frac{\sqrt{3}}{2}M_{2,y'_2,o} - \frac{1}{2}M_{3,x'_3,o} - \frac{\sqrt{3}}{2}M_{3,y'_3,o} \quad (144)$$

$$0 = M_{1,y,o} + M_{2,y,o} + M_{3,y,o} \quad (145)$$

$$0 = M_{1,y,o} - \frac{\sqrt{3}}{2}M_{2,x'_2,o} - \frac{1}{2}M_{2,y'_2,o} + \frac{\sqrt{3}}{2}M_{3,x'_3,o} - \frac{1}{2}M_{3,y'_3,o} \quad (146)$$

$$0 = M_{1,z,o} + M_{2,z,o} + M_{3,z,o} \quad (147)$$

It is now also possible to copy earlier derived formula's if the rotation axis is changed.

The formulas that we copy:

$$u_{1y} = \frac{1}{EI_x} \left(-\left(h_1 \frac{1}{4}z^2 - \frac{1}{6}z^3\right)F_{1,y,2} - \int \int u_{1y}(z)F_{1,z,2}ds^2 + \frac{1}{2h_1}z^2 \int u_{1y}(h_1)F_{1,z,2}ds + \frac{1}{2h_1}z^2 EI_{x1} \theta_x \right) \quad (148)$$

$$u_{1x} = -\frac{1}{EI_{y'_2}} \left(\left(h_1 \frac{1}{4}z^2 - \frac{1}{6}z^3\right)F_{1,x,2} + \int \int u_{1x}(z)F_{1,z,2}ds \right) - \frac{1}{2h_1}z^2 \int u_{1x}(h_1)F_{1,z,2}ds + \frac{1}{2h_1}z^2 EI_y \theta_y \quad (149)$$

$$\theta_z = \frac{1}{GJ_1} \left(-M_{z,E}h_1 + \int (u_{1y}F_{1,x,2} - u_{1x}(z)F_{1,y,2})ds \right) \quad (150)$$

$$M_{z,E} = M_{1,z,o} + LF_{1,y,2} \quad (151)$$

$$\theta_z = \frac{1}{GJ_1} \left(-h_1(M_{1,z,o} + LF_{1,y,2}) + \int (u_{1y}(z)F_{1,x,2} - u_{1x}(z)F_{1,y,2})ds \right) \quad (152)$$

Rotating them to beam 2 gives:

$$u_{2,y'_2} = \frac{1}{EI_{x'_2}} \left(-\left(h_1 \frac{1}{4} z^2 - \frac{1}{6} z^3\right) F_{2,y'_2,2} - \int \int u_{2,y'_2}(z) F_{2,z,2} ds^2 + \frac{1}{2h_1} z^2 \int u_{2,y'_2}(h_1) F_{2,z,2} ds + \frac{1}{2h_1} z^2 EI_{x_2} \theta_x \right) \quad (153)$$

$$u_{2,x'_2} = -\frac{1}{EI_{y'_2}} \left(\left(h_1 \frac{1}{4} z^2 - \frac{1}{6} z^3\right) F_{2,x'_2,2} + \int \int u_{2,x'_2}(z) F_{2,z,2} ds \right) - \frac{1}{2h_1} z^2 \int u_{2,x'_2}(h_1) F_{2,z,2} ds + \frac{1}{2h_1} z^2 EI_{y_2} \theta_y \quad (154)$$

$$\theta_z = \frac{1}{GJ_2} \left(-M_{z,E} h_1 + \int (u_{2,y'_2} F_{2,y'_2,2} - u_{2,x'_2}(z) F_{2,y'_2,2}) ds \right) \quad (155)$$

$$M_{z,E} = M_{2z,O} + LF_{2,y'_2,2} \quad (156)$$

$$\theta_z = \frac{1}{GJ_2} \left(-h_1 (M_{2z,O} + LF_{2,y'_2,2}) + \int (u_{2,y'_2}(z) F_{2,y'_2,2} - u_{2,x'_2}(z) F_{2,y'_2,2}) ds \right) \quad (157)$$

And rotating them to beam 3 gives:

$$u_{3,y'_2} = \frac{1}{EI_{x'_3}} \left(-\left(h_1 \frac{1}{4} z^2 - \frac{1}{6} z^3\right) F_{3,y'_2,2} - \int \int u_{3,y'_2}(z) F_{3,z,2} ds^2 + \frac{1}{2h_1} z^2 \int u_{3,y'_2}(h_1) F_{3,z,2} ds + \frac{1}{2h_1} z^2 EI_{x_3} \theta_x \right) \quad (158)$$

$$u_{3,x'_2} = -\frac{1}{EI_{y'_3}} \left(\left(h_1 \frac{1}{4} z^2 - \frac{1}{6} z^3\right) F_{3,x'_2,2} + \int \int u_{3,x'_2}(z) F_{3,z,2} ds \right) - \frac{1}{2h_1} z^2 \int u_{3,x'_2}(h_1) F_{3,z,2} ds + \frac{1}{2h_1} z^2 EI_{y_3} \theta_y \quad (159)$$

$$\theta_z = \frac{1}{GJ_3} \left(-M_{z,E} h_1 + \int (u_{3,y'_2}(z) F_{3,y'_2,2} - u_{3,x'_2}(z) F_{3,y'_2,2}) ds \right) \quad (160)$$

$$M_{z,E} = M_{3z,O} + LF_{3,y'_2,2} \quad (161)$$

$$\theta_z = \frac{1}{GJ_3} \left(-h_1 (M_{3z,O} + LF_{3,y'_2,2}) + \int (u_{3,y'_2}(z) F_{3,y'_2,2} - u_{3,x'_2}(z) F_{3,y'_2,2}) ds \right) \quad (162)$$

If $\theta_x = 0$, $\theta_y = 0$ and we can neglect the integral terms. Then for beam 1 we get:

$$u_{1,x_2}(z) = -\frac{1}{EI_{y_1}} \left(h_1 \frac{1}{4} z^2 - \frac{1}{6} z^3 \right) F_{1,x,2} \quad (163)$$

$$u_{1,y_2}(z) = -\frac{1}{EI_{x_1}} \left(h_1 \frac{1}{4} z^2 - \frac{1}{6} z^3 \right) F_{1,y,2} \quad (164)$$

$$\theta_z = \frac{1}{GJ_1} \left(-h_1 (M_{2z,O} + LF_{1,y,2}) \right) \quad (165)$$

We also have for beam 2:

$$u_{2,x'_2}(z) = -\frac{1}{EI_{y,2}} \left(h_1 \frac{1}{4} z^2 - \frac{1}{6} z^3 \right) F_{2,x'_2,2} \quad (166)$$

$$u_{2,y'_2}(z) = -\frac{1}{EI_{x,2}} \left(h_1 \frac{1}{4} z^2 - \frac{1}{6} z^3 \right) F_{2,y'_2,2} \quad (167)$$

$$\theta_z = \frac{1}{GJ_2} \left(-h_1 (M_{2z,O} + LF_{2,y'_2,2}) \right) \quad (168)$$

And for beam 3 we get:

$$u_{3,x'_3}(z) = -\frac{1}{EI_{y,3}} \left(h_1 \frac{1}{4} z^2 - \frac{1}{6} z^3 \right) F_{3,x'_3,2} \quad (169)$$

$$u_{3,y'_3}(z) = -\frac{1}{EI_{x,3}} \left(h_1 \frac{1}{4} z^2 - \frac{1}{6} z^3 \right) F_{3,y'_3,2} \quad (170)$$

$$\theta_z = \frac{1}{GJ_3} \left(-h_1 (M_{3z,O} + LF_{3,y'_3,2}) \right) \quad (171)$$

If the following boundary conditions are applied on on $u_{x'_2}$:

$$u_{2,x'_2}(h_1) = \Delta x'_2 - 2L \sin\left(\frac{\theta_z}{2}\right) \sin\left(\frac{\theta_z}{2}\right) + L \sin(\theta_y) \quad (172)$$

$$u_{2,x'_2}(h_1) = -\frac{1}{EI_{x,2}} \left(\frac{1}{4} h_1^3 - \frac{1}{6} h_1^3 \right) \quad (173)$$

then:

$$F_{2_{x',2}} = -\frac{12EI_{x,2}}{h_1^3}(\Delta x'_2 - 2L \sin(\frac{\theta_z}{2}) \sin(\frac{\theta_z}{2})) \approx -\frac{12EI_{x,2}}{h_1^3}(\Delta x'_2 + \frac{L}{2}\theta_z^2) \quad (174)$$

If the following boundary conditions are applied on on $u_{y'_2}$:

$$u_{2_{y'_2}}(h_1) = \Delta y'_2 + 2L \cos(\frac{\theta_z}{2}) \sin(\frac{\theta_z}{2}) + L \sin(\theta_x) \quad (175)$$

$$u_{2_{y'_2}}(h_1) = -\frac{1}{EI_{x,2}}(\frac{1}{4}h_1^3 - \frac{1}{6}h_1^3) \quad (176)$$

$$(177)$$

then:

$$F_{2_{y'_2,2}} = -\frac{12EI_{x,2}}{h_1^3}(\Delta y'_2 + 2L \cos(\frac{\theta_z}{2}) \sin(\frac{\theta_z}{2})) \approx -\frac{12EI_{x,2}}{h_1^3}(\Delta y'_2 + L\theta_z) \quad (178)$$

By taking the same steps the following equations for beam 2 and 3 can also be derived:

$$F_{2_{x,2}} = -\frac{12EI_{x,1}}{h_1^3}(\Delta x'_2 - 2L \sin(\frac{\theta_z}{2}) \sin(\frac{\theta_z}{2})) \approx -\frac{12EI_{x,1}}{h_1^3}(\Delta x'_2 + \frac{L}{2}\theta_z^2) \quad (179)$$

$$F_{2_{y,2}} = -\frac{12EI_{x,1}}{h_1^3}(\Delta y'_2 + 2L \cos(\frac{\theta_z}{2}) \sin(\frac{\theta_z}{2})) \approx -\frac{12EI_{x,1}}{h_1^3}(\Delta y'_2 + L\theta_z) \quad (180)$$

$$F_{3_{x',3}} = -\frac{12EI_{x,3}}{h_1^3}(\Delta x'_3 - 2L \sin(\frac{\theta_z}{2}) \sin(\frac{\theta_z}{2})) \approx -\frac{12EI_{x,3}}{h_1^3}(\Delta x'_3 + \frac{L}{2}\theta_z^2) \quad (181)$$

$$F_{3_{y',3,2}} = -\frac{12EI_{x,3}}{h_1^3}(\Delta y_1 + 2L \cos(\frac{\theta_z}{2}) \sin(\frac{\theta_z}{2})) \approx -\frac{12EI_{x,3}}{h_1^3}(\Delta y'_3 + L\theta_z) \quad (182)$$

With the earlier mentioned equations :

$$0 = F_{1_{x,o}} - \frac{1}{2}F'_{2_{x,o}} + \frac{\sqrt{3}}{2}F'_{2_{y,o}} - \frac{1}{2}F'_{3_{x,o}} - \frac{\sqrt{3}}{2}F'_{3_{y,o}} \quad (183)$$

$$0 = F_{1_{y,o}} - \frac{\sqrt{3}}{2}F'_{2_{x,o}} - \frac{1}{2}F'_{2_{y,o}} + \frac{\sqrt{3}}{2}F'_{3_{x,o}} - \frac{1}{2}F'_{3_{y,o}} \quad (184)$$

$$F_{1_{x,2}} = -F_{1_{x,o}} \approx -\frac{12EI_{y,1}}{h_1^3}(\Delta x + \frac{L}{2}\theta_z^2) \quad (185)$$

$$F_{2_{x',2}} = -F_{2_{x',o}} \approx -\frac{12EI_{y,2}}{h_1^3}(\Delta x'_2 + \frac{L}{2}\theta_z^2) \quad (186)$$

$$F_{3_{x',3,2}} = -F_{3_{x',o}} \approx -\frac{12EI_{y,3}}{h_1^3}(\Delta x'_3 + \frac{L}{2}\theta_z^2) \quad (187)$$

$$F_{1_{y,2}} = -F_{1_{y,o}} \approx -\frac{12EI_{x,1}}{h_1^3}(\Delta y + L\theta_z) \quad (188)$$

$$F_{2_{y'_2,2}} = -F_{2_{y',o}} \approx -\frac{12EI_{x,2}}{h_1^3}(\Delta y'_2 + L\theta_z) \quad (189)$$

$$F_{3_{y'_3,2}} = -F_{3_{y',o}} \approx -\frac{12EI_{x,3}}{h_1^3}(\Delta y'_3 + L\theta_z) \quad (190)$$

It can be derived that:

$$0 = \frac{12EI_{x,1}}{h_1^3}(\Delta y + L\theta_z) - \frac{\sqrt{3}}{2} \frac{12EI_{y,2}}{h_1^3}(\Delta x'_2 + \frac{L}{2}\theta_z^2) - \frac{1}{2} \frac{12EI_{x,2}}{h_1^3}(\Delta y'_2 + L\theta_z) + \frac{\sqrt{3}}{2} \frac{12EI_{y,3}}{h_1^3}(\Delta x'_3 + \frac{L}{2}\theta_z^2) - \frac{1}{2} \frac{12EI_{x,3}}{h_1^3}(\Delta y'_3 + L\theta_z) \quad (191)$$

and

$$0 = \frac{12EI_{y1}}{h_1^3}(\Delta x + \frac{L}{2}\theta_z^2) - \frac{1}{2} \frac{12EI_{y,2}}{h_1^3}(\Delta x'_2 + \frac{L}{2}\theta_z^2) + \frac{\sqrt{3}}{2} \frac{12EI_{x,2}}{h_1^3}(\Delta y'_2 + L\theta_z) - \frac{1}{2} \frac{12EI_{y,3}}{h_1^3}(\Delta x'_3 + \frac{L}{2}\theta_z^2) - \frac{\sqrt{3}}{2} \frac{12EI_{x,3}}{h_1^3}(\Delta y'_3 + L\theta_z) \quad (192)$$

$$(193)$$

and if we use:

$$\begin{pmatrix} \Delta x'_2 \\ \Delta y'_2 \\ \Delta x'_3 \\ \Delta y'_3 \end{pmatrix} = \begin{pmatrix} -\frac{1}{2}\Delta x \frac{\sqrt{3}}{2}\Delta y \\ -\frac{\sqrt{3}}{2}\Delta x - \frac{1}{2}\Delta y \\ -\frac{1}{2}\Delta x - \frac{\sqrt{3}}{2}\Delta y \\ \frac{\sqrt{3}}{2}\Delta x - \frac{1}{2}\Delta y \end{pmatrix} \quad (194)$$

$$(195)$$

then it follows that:

$$\Delta x = \frac{4I_{x,1}(L\theta_z + \Delta y) + \sqrt{3}(I_{y,3} - I_{y,2})L\theta_z^2 - 2(I_{x,2} + I_{x,3})L\theta_z + (I_{x,2} + I_{x,3} + 3(I_{y,2} + I_{y,3}))\Delta y}{\sqrt{3}(I_{x,2} - I_{x,3} - I_{y,2} + I_{y,3})} \quad (196)$$

$$\Delta y = \frac{(2I_{y,1} - I_{y,2} - I_{y,3})L\theta_z^2 + 2\sqrt{3}(I_{x,2} - I_{x,3})L\theta_z + (3I_{x,2} + 3I_{x,3} + 4I_{y,1} + I_{y,2} + I_{y,3})\Delta x}{\sqrt{3}(I_{x,2} - I_{x,3} - I_{y,2} + I_{y,3})} \quad (197)$$

Now determine Δy and Δx can be determined:

$$\begin{aligned} \Delta y &= (L(-I_{x,1}(3I_{x,2} + 3I_{x,3} + 4I_{y,1} + I_{y,2} + I_{y,3}) \sin(\theta_z) + I_{x,3}(2I_{y,1} - I_{y,2} + 2I_{y,3}) \sin(\theta_z) - 3\sqrt{3}I_{y,1}(I_{y,2} - I_{y,3})(\cos(\theta_z) - 1) + (-\sqrt{3})I_{x,3}(I_{y,1} \\ &+ I_{y,2} - 2I_{y,3})(\cos(\theta_z) - 1) + I_{x,2}((6I_{x,3} + 2(I_{y,1} + I_{y,2}) - I_{y,3}) \sin(\theta_z) + \sqrt{3}(I_{y,1} - 2I_{y,2} + I_{y,3})(\cos(\theta_z) - 1)))) / (I_{x,3}I_{y,1} \\ &+ 3I_{y,2}I_{y,1} + I_{x,3}I_{y,2} + (4I_{x,3} + 3(I_{y,1} + I_{y,2}))I_{y,3} + I_{x,1}(3I_{x,2} + 3I_{x,3} + 4I_{y,1} + I_{y,2} + I_{y,3}) + I_{x,2}(3I_{x,3} + I_{y,1} + 4I_{y,2} + I_{y,3})) \\ \Delta x &= (2L((-I_{x,3}I_{y,1} - 3I_{y,2}I_{y,1} - I_{x,3}I_{y,2} + (2I_{x,3} - 3I_{y,1} + 6I_{y,2})I_{y,3} + 2I_{x,1}(-2I_{y,1} + I_{y,2} + I_{y,3}) - I_{x,2}(I_{y,1} - 2I_{y,2} + I_{y,3}))) \sin(\frac{\theta_z}{2})^2 \\ &+ \sqrt{3}(I_{x,1}(-3I_{x,2} + 3I_{x,3} + I_{y,2} - I_{y,3}) - I_{x,2}(2I_{y,2} + I_{y,3}) + I_{x,3}(I_{y,2} + 2I_{y,3})) \sin(\frac{\theta_z}{2}) \cos(\frac{\theta_z}{2})) / (I_{x,3}I_{y,1} + 3I_{y,2}I_{y,1} \\ &+ I_{x,3}I_{y,2} + (4I_{x,3} + 3(I_{y,1} + I_{y,2}))I_{y,3} + I_{x,1}(3I_{x,2} + 3I_{x,3} + 4I_{y,1} + I_{y,2} + I_{y,3}) + I_{x,2}(3I_{x,3} + I_{y,1} + 4I_{y,2} + I_{y,3})) \end{aligned}$$

From these equations it can be seen that if $I_{x,1} = I_{x,2} = I_{x,3}$ and $I_{y,1} = I_{y,2} = I_{y,3}$ that then $\Delta y = 0$ and $\Delta x = 0$

It is now derived that the expressions below are only dependent on θ_z :

$$F_{1_{x',2}} = -F_{1_{x',o}} \approx -\frac{12EI_{y1}}{h_1^3}(\Delta x + \frac{L}{2}\theta_z^2) \quad (198)$$

$$F_{2_{x',2}} = -F_{2_{x',o}} \approx -\frac{12EI_{y,2}}{h_1^3}(\Delta x'_2 + \frac{L}{2}\theta_z^2) \quad (199)$$

$$F_{3_{x',2}} = -F_{3_{x',o}} \approx -\frac{12EI_{y,3}}{h_1^3}(\Delta x'_3 + \frac{L}{2}\theta_z^2) \quad (200)$$

$$F_{1_{y',2}} = -F_{1_{y',o}} \approx -\frac{12EI_{x1}}{h_1^3}(\Delta y + L\theta_z) \quad (201)$$

$$F_{2_{y',2}} = -F_{2_{y',o}} \approx -\frac{12EI_{x,2}}{h_1^3}(\Delta y'_2 + L\theta_z) \quad (202)$$

$$F_{3_{y',2}} = -F_{3_{y',o}} \approx -\frac{12EI_{x,3}}{h_1^3}(\Delta y'_3 + L\theta_z) \quad (203)$$

Lets now take a look at the equations for the moment about z.

With the following equations :

$$M_{z,o} = M_{1_{z,o}} + M_{2_{z,o}} + M_{3_{z,o}} \quad (204)$$

$$\theta_z = \frac{1}{GJ_1} (-h_1 (M_{1_{z,o}} + LF_{1_{y,2}})) \quad (205)$$

$$\theta_z = \frac{1}{GJ_2} (-h_1 (M_{2_{z,o}} + LF_{2_{y',2}})) \quad (206)$$

$$\theta_z = \frac{1}{GJ_3} (-h_1 (M_{3_{z,o}} + LF_{3_{y',2}})) \quad (207)$$

We can derive:

$$M_{1_{z,o}} = (LF_{1_{y,2}} - \frac{1}{h_1} GJ_1 \theta_z) \quad (208)$$

$$M_{2_{z,o}} = (LF_{2_{y',2}} - \frac{1}{h_1} GJ_2 \theta_z) \quad (209)$$

$$M_{3_{z,o}} = (LF_{3_{y',2}} - \frac{1}{h_1} GJ_3 \theta_z) \quad (210)$$

$$M_{z,o} = (LF_{1_{y,2}} - \frac{1}{h_1} GJ_1 \theta_z) + (LF_{2_{y',2}} - \frac{1}{h_1} GJ_2 \theta_z) + (LF_{3_{y',2}} - \frac{1}{h_1} GJ_3 \theta_z) \quad (211)$$

$$\theta_z = h_1 \frac{-M_{z,o} + LF_{1_{y,2}} + LF_{2_{y',2}} + LF_{3_{y',2}}}{GJ_1 + GJ_2 + GJ_3} \quad (212)$$

In which we can substitute equation 198-203 to get an expression for M_z that only depends on θ_z . And also the expression for θ_z that only depends on M_z can be easily derived from this.

B Stiffness Matrix $C_{O,O}$

In this appendix, the stiffness matrix, that is derived in section 3.1.7 is given. If the Stiffness matrix $C_{O,O}$ is given by:

$$C_{O,O} = \begin{pmatrix} A_1 & A_2 & A_3 & A_4 & A_5 & A_6 \\ B_1 & B_2 & B_3 & B_4 & B_5 & B_6 \\ C_1 & C_2 & C_3 & C_4 & C_5 & C_6 \\ D_1 & D_2 & D_3 & D_4 & D_5 & D_6 \\ E_1 & E_2 & E_3 & E_4 & E_5 & E_6 \\ F_1 & F_2 & F_3 & F_4 & F_5 & F_6 \end{pmatrix} \quad (213)$$

Then the components are given by:

$$A_1 = \frac{3E(3I_{x,2} + 3I_{x,3} + 4I_{y,1} + I_{y,2} + I_{y,3})}{h^3} \quad (214)$$

$$B_1 = \frac{3\sqrt{3}E(I_{x,2} - I_{x,3} - I_{y,2} + I_{y,3})}{h^3} \quad (215)$$

$$C_1 = 0 \quad (216)$$

$$D_1 = \frac{3\sqrt{3}E(I_{x,2} - I_{x,3} - I_{y,2} + I_{y,3})}{h^2} \quad (217)$$

$$E_1 = -\frac{3E(3I_{x,2} + 3I_{x,3} + 4I_{y,1} + I_{y,2} + I_{y,3})}{h^2} \quad (218)$$

$$F_1 = \frac{6\sqrt{3}E(I_{x,3} - I_{x,2})L}{h^3} \quad (219)$$

$$A_2 = \frac{3\sqrt{3}E(I_{x,2} - I_{x,3} - I_{y,2} + I_{y,3})}{h^3} \quad (220)$$

$$B_2 = \frac{3E(4I_{x,1} + I_{x,2} + I_{x,3} + 3(I_{y,2} + I_{y,3}))}{h^3} \quad (221)$$

$$C_2 = 0 \quad (222)$$

$$D_2 = \frac{3E(4I_{x,1} + I_{x,2} + I_{x,3} + 3(I_{y,2} + I_{y,3}))}{h^2} \quad (223)$$

$$E_2 = \frac{3\sqrt{3}E(-I_{x,2} + I_{x,3} + I_{y,2} - I_{y,3})}{h^2} \quad (224)$$

$$F_2 = \frac{6E(2I_{x,1} - I_{x,2} - I_{x,3})L}{h^3} \quad (225)$$

$$A_3 = 0 \quad (226)$$

$$B_3 = 0 \quad (227)$$

$$C_3 = \frac{2(A_1 + A_2 + A_3)E}{h} \quad (228)$$

$$D_3 = \frac{\sqrt{3}(A_3 - A_2)EL}{h} \quad (229)$$

$$E_3 = \frac{(2A_1 - A_2 - A_3)EL}{h} \quad (230)$$

$$F_3 = 0 \quad (231)$$

$$A_4 = \frac{3\sqrt{3}E(I_{x,2} - I_{x,3})}{2h^2} \quad (232)$$

$$B_4 = \frac{3E(4I_{x,1} + I_{x,2} + I_{x,3})}{2h^2} \quad (233)$$

$$C_4 = \frac{(2A_1 - (1 + \sqrt{3})A_2 + (-1 + \sqrt{3})A_3)EL}{h} \quad (234)$$

$$D_4 = \frac{2((3 + \sqrt{3})A_2 - (-3 + \sqrt{3})A_3)EL^2 + 3E(8I_{x,1} + 2I_{x,2} + 2I_{x,3} + I_{y,2} + I_{y,3})}{4h} \quad (235)$$

$$E_4 = \frac{E(2(4A_1 + \sqrt{3}A_2 + A_2 - \sqrt{3}A_3 + A_3)L^2 - 6\sqrt{3}I_{x,2} + 6\sqrt{3}I_{x,3} + \sqrt{3}I_{y,2} - \sqrt{3}I_{y,3})}{4h} \quad (236)$$

$$F_4 = \frac{3E(2I_{x,1} - I_{x,2} - I_{x,3})L}{h^2} \quad (237)$$

$$A_5 = -\frac{9E(I_{x,2} + I_{x,3})}{2h^2} \quad (238)$$

$$B_5 = \frac{3\sqrt{3}E(I_{x,3} - I_{x,2})}{2h^2} \quad (239)$$

$$C_5 = \frac{(2A_1 + (-1 + \sqrt{3})A_2 - (1 + \sqrt{3})A_3)EL}{h} \quad (240)$$

$$D_5 = -\frac{E(2((3 + \sqrt{3})A_3 - (-3 + \sqrt{3})A_2)L^2 + 6\sqrt{3}I_{x,2} - 6\sqrt{3}I_{x,3} - \sqrt{3}I_{y,2} + \sqrt{3}I_{y,3})}{4h} \quad (241)$$

$$E_5 = \frac{E(2(4A_1 - \sqrt{3}A_2 + A_2 + \sqrt{3}A_3 + A_3)L^2 + 18I_{x,2} + 18I_{x,3} + 4I_{y,1} + I_{y,2} + I_{y,3})}{4h} \quad (242)$$

$$F_5 = \frac{3\sqrt{3}E(I_{x,2} - I_{x,3})L}{h^2} \quad (243)$$

$$A_6 = \frac{6\sqrt{3}E(I_{x,3} - I_{x,2})L}{h^3} \quad (244)$$

$$B_6 = \frac{6E(2I_{x,1} - I_{x,2} - I_{x,3})L}{h^3} \quad (245)$$

$$C_6 = 0 \quad (246)$$

$$D_6 = \frac{6E(2I_{x,1} - I_{x,2} - I_{x,3})L}{h^2} \quad (247)$$

$$E_6 = \frac{6\sqrt{3}E(I_{x,2} - I_{x,3})L}{h^2} \quad (248)$$

$$F_6 = \frac{G(J_1 + J_2 + J_3)h^2 + 12E(I_{x,1} + I_{x,2} + I_{x,3})L^2}{h^3} \quad (249)$$

C Full expressions for the stresses derived from the linear model

In this appendix, the full expressions for the stresses derived from the linear model are given.

The normal stress that follows from the linear model is given by:

$$\sigma_{33} = \frac{E (Ah^2(\Delta_z + L(\theta_x + \theta_y)) + 2A(-3\Delta_x x(h-2z) + 3\Delta_y y(h-2z) + 3\theta_z Ly(h-2z) + h(h-3z)(\theta_y x + \theta_x y))}{Ah^3} \quad (250)$$

The shear stress that follows from the linear model is given by:

$$\sigma_{13} = \sigma_{31} \frac{2G\theta_{z,y}}{h} \quad (251)$$

The equivalent stress that follows from the linear model is given by:

$$\sigma_{eq} = \frac{1}{\sqrt{2}} \sqrt{6\sigma_{13}^2 + 2\sigma_{33}^2} \quad (252)$$